UNIVERSITÀ
DEGLI STUDI
DI PADOVA

Dipartimento di Ingegneria Industriale
Dipartimento di Ingegneria dell'Informazione

Corso di Laurea Magistrale in Ingegneria dell'energia Elettrica

TESI DI LAUREA MAGISTRALE IN
INGEGNERIA DELL'ENERGIA ELETTRICA

Measurement of strain on a wind turbine blade by optical fibre sensing

RELATORE: Prof. Luca Palmieri

LAUREANDO: Mattia Lazzaro

ANNO ACCADEMICO 2018-19

UNIVERSITÀ DEGLI STUDI DI PADOVA

Department of Industrial Engineering

Department of Information Engineering

Master Degree in Electrical Energy Engineering

Master Degree thesis:

Measurement of strain on a wind turbine blade by optical fibre sensing

Supervisor: Prof. Palmieri Luca

Tutor at Guangzhou University: Prof. Zhu Pingyu

Graduand: Lazzaro Mattia

Matriculation number: 1140464

ACADEMIC YEAR: 2018/2019

Abstract

Wind power is becoming day after day an important source of energy, especially once converted into electrical power. Monitoring wind turbines conditions and predicting possible problems is important, not only during their working time. A massive production of wind turbine blades entails the presence of a fast and inexpensive way of manufacturing and testing. Being potentially exposed to strong wind currents, the blades must be harmless when in action (even when they are *cut out*), to preserve their and their surrounding safety.

Several parameters must be fixed to have a performant and safe blade model. Mechanical properties are important; therefore it is essential to take precise measurements of strain, when the component is under stress. Several instruments can measure it, but features and results are different.

This thesis is focussed on sensing of wind turbine blade, especially on optical fibre sensing (OFSs), above all distributed optical fibre sensing (DOFSs). There are different kinds of OFSs based on different kinds of physical processes (for example Brillouin, Raman, Rayleigh scattering, depending on the sensor used). The field of DOFSs has born from just a theoretical concept in the beginning of the 1980s and has reached an extensive usage in these years. The research is very active and promising.

Sommario

La tesi è stata svolta presso l'Università di Guangzhou, Cina, in collaborazione con l'azienda Zhuzhou Times New Material Technology Co., Ltd. (株洲时代新材料科技股份有限公司), che ha messo a disposizione per i test la pala eolica.

Vista l'importanza che sta acquistando oggi l'energia eolica, in particolare in stati come la Cina, che investe molto per migliorare la qualità dell'aria del paese e che comunque ha vaste zone offshore ed interne adatte all'installazione di impianti eolici, è molto importante che la produzione dei componenti, che aumenta in quantità molto rapidamente, sia di ottima qualità.

Focalizzando l'attenzione sulla pala eolica, è essenziale che essa sia resistente all'esposizione a forti correnti d'aria durante il funzionamento o comunque a possibili situazioni anomale. I parametri meccanici sono sorvegliati speciali e devono rientrare entro determinate soglie. Per questo motivo la pala è sottoposta a vari test iniziali (prove di fatica di varia durata e con differenti metodologie) che possono provare il suo corretto funzionamento (o meno). Per ottenere statistiche e dati si possono usare sensori di varie famiglie: elettrici o in fibra ottica, ad esempio.

La tesi si occupa inizialmente di introdurre quali sono i parametri meccanici da essere controllati e quali possono essere le cause di rottura della pala eolica (in base anche al materiale di cui è costituita). In un secondo momento, confronta le varie tecnologie esistenti per la misurazione dei parametri. Quindi si introduce il metodo di misurazione basato sulle fibre ottiche.

I sensori in fibra ottica oggi sono principalmente usati nel settore idrogeologico e di monitoraggio strutturale, tuttavia esistono molteplici applicazioni di altro tipo. Infatti, viste le caratteristiche fisiche che permettono ai sensori di essere posizionati anche nei luoghi più critici, l'OFS (Optical Fibre Sensing) risulta un buon compromesso.

Anche i sensori in fibra ottica si possono suddividere in diverse categorie e l'ottenimento delle misurazioni avviene analizzando diversi tipi di processi fisici (ad esempio Brillouin, Raman, Rayleigh scattering, a seconda del sensore utilizzato). Per quanto riguarda questo elaborato si sono usati sensori distribuiti (DOFS) e FBG.

Le fibre ottiche, conosciute dalla maggior parte della popolazione d'oggi come strumenti di telecomunicazione, hanno assunto negli ultimi 25 anni un ruolo sempre più importante nel campo di applicazione della sensoristica. La ricerca è molto attiva e promettente.

Contents

List of figures

List of tables

List of abbreviations

ASEs	Amplified Spontaneous Emissions
BOTDA	Brillouin Optical-Time Domain Analysis
BOTDR	Brillouin Optical-Time Domain Reflectometry
C-OFDR	Coherent-OFDR
CFRP	Carbon Fibre Reinforced Polymer
CW	Continuous Wave
DOFS	Distributed Optical Fibre Sensor
DPP-BOTDA	Differential Pulse-width Pair BOTDA
DTS	Distributed Temperature Sensor
E_{ph}	Energy of the photons
FBG	Fiber Bragg Grating
FMCW	Frequency-Modulated Continuous-Wave
GFRP	Glass Fibre Reinforced Polymer
I-OFDR	Incoherent OFDR
k_bT	Unit thermal energy
k_b	Boltzmann constant
LA	Longitudinal Acoustic
LE	Leading Edge
MEMSs	Micro-Electro Mechanical Systems
NA	Numerical Aperture
OFDR	Optical Frequency-Domain Reflectometry
OFS	Optical Fibre Sensor
ODPA-BOTDA	Optical-Differential Parametric Amplification
OTDR	Optical Time-Domain Reflectometry
PS	Pressure Side
SBS	Stimulated Brillouin Scattering
SF-BOTDA	Sweep-Free BOTDA
SHM	Structural Health Monitoring
SpBS	Spontaneous Brillouin Scattering
SPM	Self-Phase Modulation

SRS	Stimulated Raman Scattering
SS	Suction Side
TA	Transverse Acoustic
TE	Trailing Edge
V	Normalised frequency
WT	Wind Turbine

Chapter 1

1 - Introduction

WTs (Wind turbines) are becoming more and more frequent in the lands all over the world, offering an additional and clean source of electric power. Increased presence of wind power supplies renewable energy and reduces dependence on fossil fuels. Countries are sponsoring the construction of wind on-shore and offshore power plants and the cost is becoming competitive when compared to other power plants (especially if we think that the cost of fuel for a WT is null).

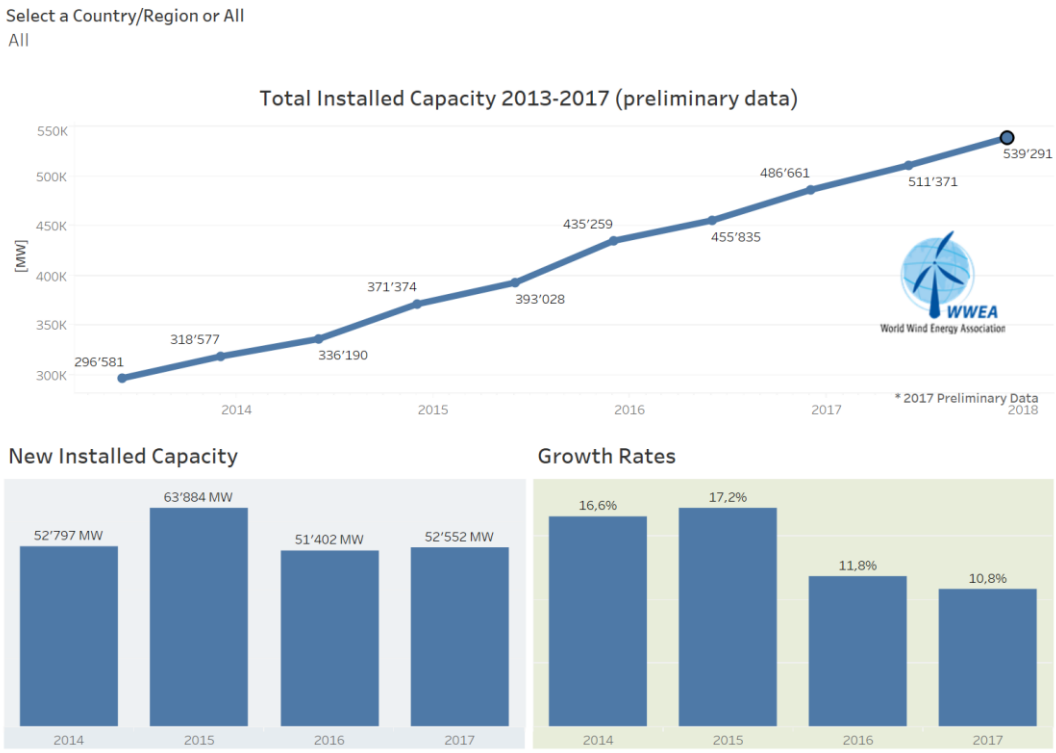

Figure 1.1: Total Installed Capacity of Wind Power Plants 2013-2017, World Wind Energy Association (preliminary data) [1].

As consequence, WTs have become larger, and the forces acting on the blades have increased, leading to stronger mechanical stresses and higher possibility of fatigue failures such as broken WT blades or tower strikes. This leads the industry to have a higher focus on creating an efficient and resistant model of WTs components and on Structural Health Monitoring (SHM), to prevent failure and reduce maintenance costs.

The technology has led to several instruments that can help to create suitable components of WT. Instruments that can measure strain, temperature and many other physical relevant quantities. They are for example electrical gauges, acoustic emission sensors, optical fibre sensors, wireless strain sensors. The instrument, as usually happens in engineering, will be chosen according to economic factors and specific requirements.

In the WT blade study case (on which the thesis is focussing), the aim of this elaborate is proving that OFSs (Optical Fibre Sensors) are a good choice, and especially that the BOTDA (Brillouin Optical Time Domain Analysis) OFS is the best compromise. A longer dissertation will be treated in other sections of the thesis.

1.1 - Wind turbine blade: main features

The perspectives of application and development of wind energy technology depend also on the trustworthiness and lifetime of WTs.

WT blade is one of the basic components in WTs, as it is the only member able to receive and transform wind energy in mechanical energy, and has primary influence on WT operation stability. WT blades are usually made of fiberglass material, to be cost effective, but they can be damaged by moisture absorption, fatigue, wind gusts or lightning strikes [2].

It is fundamental to detect the damage before the blade fails irreparably, as it could destroy the entire WT system. As said, as the size of modern blades comes bigger, their monitoring and maintenance conditions increases in importance, and strain detection is one of the most effective methods to do it.

Degradation processes in WT blades are controlled by microscale processes in the materials [3]. It is important to understand the degradation mechanisms of wind blades as a function of the blade's structure, and so forecast their life expectancy and service characteristics. Then, a possible way could be estimating the loads on the wind blades.

Figure 1.2: Example of blade's damage due to wind gusts.

1.2 - Motivation and objectives of this elaborate

During my exchange programme at Guangzhou University - Guangdong - China, Professor Zhu Pingyu and her team have first proposed me to write a thesis with topic OFS. Finally, the proposal evolved to OFS applied to a WT blade. The project has been conducted with the collaboration of Zhuzhou Times New Material Technology Co., Ltd. (株洲时代新材料科技股份有限公司), who provided us the WT blade and welcomed us for the measurements.

The motivation of the thesis is giving a solution, in terms of mechanical characteristics, for the right modelling of the blade. Is then important to find the right way to measure quantities like strain, when the blade is operating in working conditions (or, like in our case, in simulated working conditions).

The objective is to find the right measuring instrument and right way to do the measurements. More sensors will be considered and appropriate explanations are given. The thesis focusses on BOTDA system, which is predicted to be the most suitable. Finally, a complete description about the experiment and some clarifications about the results are reported.

Chapter 2

2 - Wind turbine blade's mechanical characteristics

There are several studies estimating the loads on WT blades (aerodynamic, physical loads…). However, in this work, I follow a simple model-based method introduced in the complex materials model as a boundary condition [4]. The aim of this chapter, is not giving a complete mock-up of the subject matter of the research (blade), but just let the reader understand the importance of mechanical quantities like stress, load distribution, stiffness, weight distribution, for the modelling of a blade.

2.1 - Blade model

A wind turbine blade consists of two faces (on the suction side and the pressure side), joined together, and stiffened either by one or several integral (shear) webs, linking the upper and lower parts of the blade shell or by a box beam (box spar with shell fairings), like in figure 2.1 [5].

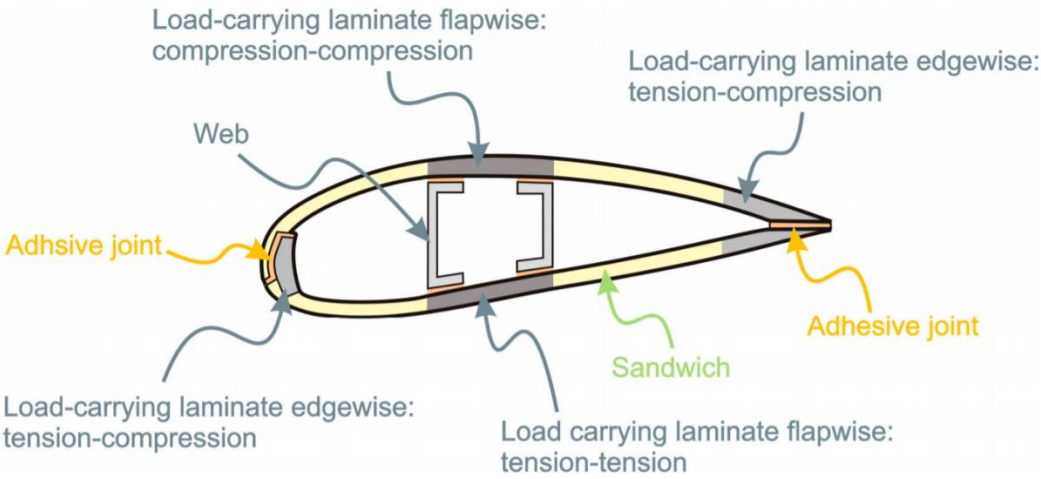

Figure 2.1: Section of a generic WT blade.

About the loads on the component's materials, one of the laminates (in the pressure side) in the main spar is vulnerable to cyclic tension-tension loads, whereas the other one (in the suction side) is vulnerable to cyclic compression-compression loads. The aeroshells, which are made of sandwich structures (honeycomb structure), are originally created to resist to the elastic buckling. The different cyclic loading conditions that are present at the various places at the blades indicate that it could be convenient to use different materials for different components and parts of the blade (see figure 2.1).

As said before, the subject matter of this research (blade) is provided by Zhuzhou Times New Material Technology Co., Ltd. (株洲时代新材料科技股份有限公司). The blade, as reported by the company, is long around 60 m (the data is not precise according to the agreement made with the company) and presents a special structure, made of wood, copper honeycomb, GFRP (Glass Fibre Reinforced Polymer), and CFRP (Carbon Fibre Reinforced Polymer). The wood is the main element: it is used

because of its lightness and its cost benefit. On the other hand, the disadvantages are the quality variations, high moisture uptake and low thermal stability of the raw fibers [5]. For this reason, the structure is combined with a copper honeycomb. The composite (honeycomb) technology has high strength and low weight, and is a way to lighten the blade framework and absorb impact energy. The combined structure covers the blade in all its extension. GFRP is employed to cover two restricted areas along the blade: the trailing edge and the leading edge. It is used because of its physical characteristics (it is stiff and strong in tension and compression). The two spar caps present in the blade and a part of the main beam are made of CFRP. CFRP is characterized by high strength-to-weight ratio and rigidity.

The increasing sizes of the WTs entails to a cheaper price of the electrical energy but harder engineering challenges. For example, a bigger size means a bigger weight of the blade; gravitational loads become then an essential point for the design. On the same time, a longer blade will deflect more: is then important focussing on its stiffness. Last, the life cycle of the turbine is expected to be longer and longer (lately, 20-25 years). It is then important planning a good sandwich/composite structure to deal with the high-cycle fatigue.

2.2 - Loads on the blade

A WT blade is a long, narrow structure, where the dominating loads are affected by aerodynamics factors and the gravity. From a macroscopic point of view, a WT blade could be seen as a simple beam structure with a crisp load profile and boundary conditions. Quantities like deflections, loads and stresses could be evaluated by using a (simplified) beam model. The results depend on the material of the blade, as GFRP (glass fibre reinforced polymers), aluminium alloy or CFRP (carbon fibre reinforced polymers), and on the length of the blade (a long blade, once exposed to a wind flow, will be more deflected than a short one). Moreover, the conception of the blade's model is function of different physical characteristics: for example, for a GFRP blade is important the deflection, because the blade could strike the tower once the turbine is in action. Is important to notice that the GFRP is today the most used, since it is a matured material, while CFRP is still too expensive and aluminium alloy is only used for small turbines.

The *beam theory* (as blade describing method) can be made at different levels of complexity, depending on the way it is used. In a simplified 1D (1-dimension) momentum theory, the maximum aerodynamic load on a blade, in the flapwise direction, can be simplified as a linear varying distributed load with vanishing load intensity at the root to a load intensity [6]. In figure 2.2, is possible to see how the wind's flow is evolving from the upstream, or $()_u$ region, to the downstream, or $()_d$ region, crossing in the middle the WT disc region, called also $()_t$ region. The speed of the wind u_i is decreasing from the upstream value u_u to the downstream value u_d. Consequence of this is an increase of the respective area A_i ($A_d > A_u$). On the other hand the pressure p_i, is constant (and equal to ambient pressure, p_∞) in the upstream and downstream region, while in the WT region changes from p_1 to p_2, because of the rotation of the WT (and its "absorption" of work).

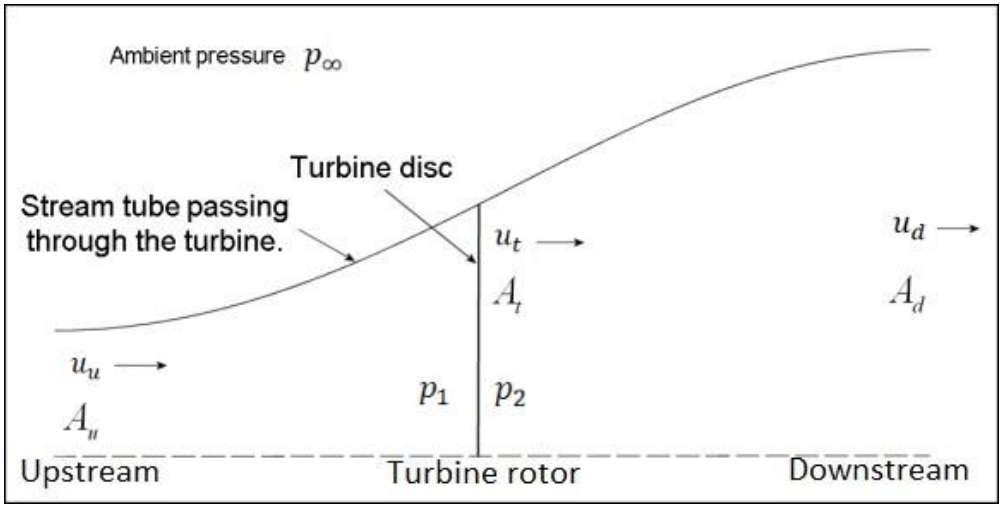

Figure 2.2: Scheme of fluid flow through a disk-shaped actuator (in this case a WT).

Considering the previous points (especially the ones who say that the pressure in the far upstream and in the far downstream is equal to the ambient pressure and the speed and pressure crossing the WT disc change continuously) and that in the far upstream u_u could be considerate equal to u_∞, is possible to write down the formulas (2.1), (2.2):

$$u_t = \frac{u_\infty + u_d}{2} \tag{2.1}$$

$$\Delta p_t = p_1 - p_2 \tag{2.2}$$

Considering then the Bernoulli Principle, we can relate the upstream, turbine rotor and downstream area by the relations (2.3), (2.4):

$$p_\infty + \frac{\rho_{air} u_\infty^2}{2} = p_1 + \frac{\rho_{air} u_t^2}{2} \tag{2.3}$$

$$p_\infty + \frac{\rho_{air} u_d^2}{2} = p_2 + \frac{\rho_{air} u_t^2}{2} \tag{2.4}$$

Operating "(2.3) – (2.4)" we obtain:

$$\Delta p_t = \frac{\rho_{air}(u_\infty^2 - u_d^2)}{2} \tag{2.5}$$

Q_t, the thrust force working on the WT rotor, is defined as $Q_t = \Delta p_t A_t$.

Defining P_t, the power taken by the WT (from wind's power), it's possible to make the following considerations.

As function of time, P_t is equal to the difference of the kinetic energy of the upstream and downstream area. The mass flow through the turbine is $\dot{m}$,

$$\dot{m} = \rho_{air} A_t u_t \tag{2.6}$$

The parameter a is:

$$a = \frac{u_\infty - u_t}{u_\infty} \tag{2.7}$$

P_t is defined as:

$$P_t = Q_t u_t = \frac{\rho_{air} A_t u_t (u_\infty^2 - u_d^2)}{2} = \frac{\rho_{air} A_t u_\infty^3 4a(1-a)^2}{2} \tag{2.8}$$

When a = 1/3, that is the Betz limit, P_t reaches its maximum value, in other words the 60% of the upstream wind power. Nowadays is possible to modify the position of the blades of the WTs, in according to the value of u_t (to reach the Betz limit).

When P_t reaches the value of P_g, the generator power, the blades position will be chosen in order to let P_t not overcome P_g. Then u_r, the rated wind speed, is set as design parameter of the blade, so that:

$$a = \begin{cases} \frac{1}{3}, & u_\infty \leq u_r \\ f(P_g;\, u_\infty), & u_\infty > u_r \end{cases} \tag{2.9}$$

$f(P_g;\, u_\infty)$ is characterized by:

$$a(1-a)^2 = \frac{P_g}{2\rho_{air} u_\infty^3 A_t} \tag{2.10}$$

From the relations (2.9), (2.10) and the definition of Q_t, Q_t can be seen as $Q_t(u_\infty)$, function of u_∞. The maximum value of Q_t is reached when $u_\infty = u_r$.

Is true that (being L the blade length):

$$Q_{tmax} = \frac{4\rho_{air} u_r^2 \pi L^2}{9} \tag{2.11}$$

This load will be distributed (for example) to three blades, with 1/3 to each one. Along the individual blade, the load intensity (load per unit length), q_x^{fw}[1], can be approximated by linear varying distribution from a vanishing value at the root to the maximum value at the blade tip given by [6]:

$$q_x^{fw} = \frac{8}{27}\rho_{air} u_R^2 \pi x \tag{2.12}$$

On the other hand, should be considered also the edgewise direction load, due to the gravity. Calling ρ_{bl}[2], the density of the material of the blade and g the gravity acceleration, is true that:

$$q_x^{ew} = \rho_{bl} A_{bl} g \tag{2.13}$$

[1] *fw* = flapwise.
[2] *bl* = blade.
[3] *ew* = edgewise.

2.3 - Stresses of the blade

In figure 2.3 is represented a simplification of a WT blade structure when exposed to a wind current. The part (a) represents the stressed parts of the blade, respectively because of the flapwise bending (vertical direction[4]) and edgewise bending (horizontal direction[5]). The part marked with green is the load carrying part contributing to the overall stiffness of the blade [6].

The part (b) is a simplified representation of the blade section, useful for the calculation of the stresses on the blade.

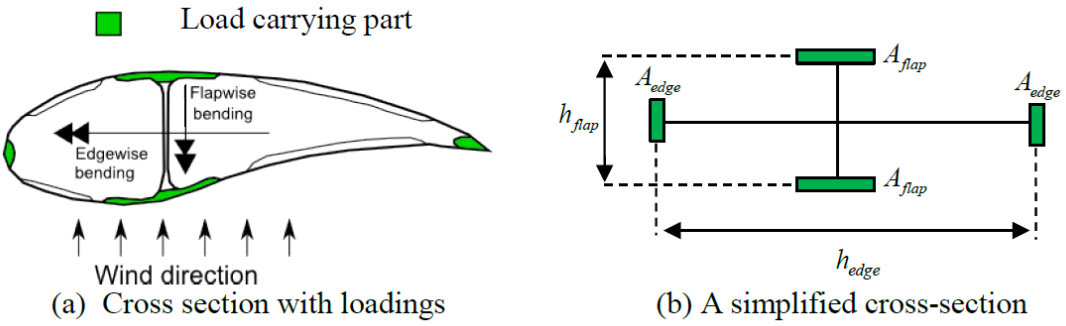

Figure 2.3: Typical wind turbine cross section and simplified cross-section [5].

Flapwise and edgewise moment can be found as:

$$M_x^{fw} = q_x^{fw}(L-x)\frac{L-x}{2} + \frac{q_L^{fw} - q_x^{fw}}{2}(L-x)\frac{2(L-x)}{3} \tag{2.14}$$

$$M_x^{ew} = \rho_{bl} A_{bl} g (L-x)\frac{L-x}{2} \tag{2.15}$$

The stress (flapwise and edgewise) can be found, using (2.14) and (2.15) and taking into account that $A_{bl} = 2(A_{fw} + A_{ew})$, as:

$$\sigma_x^{fw} = \frac{8\rho_{air} u_r^2 \pi L^3}{81 A_{fw} h_x^{fw}}(1 + x/2L)(1 - x/L)^2 \tag{2.16}$$

$$\sigma_x^{ew} = \frac{\rho_{bl} A_{bl} g L^2}{2 A_{ew} h_x^{ew}}(1 - x/L)^2 \tag{2.17}$$

In order to achieve a constant stress level, $\sigma_x^{fw} = \sigma_x^{ew} = \sigma_0$ in the blade material, it can be seen from (2.16) and (2.17) that the blade height, h_x^{fw}, and blade width, h_x^{ew}, should vary in the following way [6]:

$$\frac{h_x^{fw}}{h_0^{fw}} = \left(1 + \frac{x}{2L}\right)\left(1 - \frac{x}{L}\right)^2 \tag{2.18}$$

[4] The flapwise bending follows the vertical direction because of the wind vector (see figure 2.3).
[5] The edgewise bending follows the horizontal direction because the gravity factors influences the blade's mechanical parameters, especially when the turbine is rotating (see figure 2.3).

$$\frac{h_x^{ew}}{h_0^{ew}} = \left(1 - \frac{x}{L}\right)^2 \tag{2.19}$$

(2.18) and (2.19) give a simplified mathematical model (based on the material strength) for modelling a blade. By the way, to achieve the final characterization of a WT blade there are more requisites (like aerodynamic); this make the evaluations more difficult and quite different to the one we are examining in this chapter. L is always known, as length of the blade, while h_0^{fw} and h_0^{ew}, the biggest value points who represent the characteristic shape of the blade, can be found, comparing more (blade) geometries by the following linear function of the length L [6]:

$$h_o^{fw} = 0.066L - 0.369m \tag{2.20}$$
$$h_0^{ew} = 0.130L + 0.082m \tag{2.21}$$

From (2.18), (2.19), (2.20), (2.21), we can get the graphs of figure 2.4.

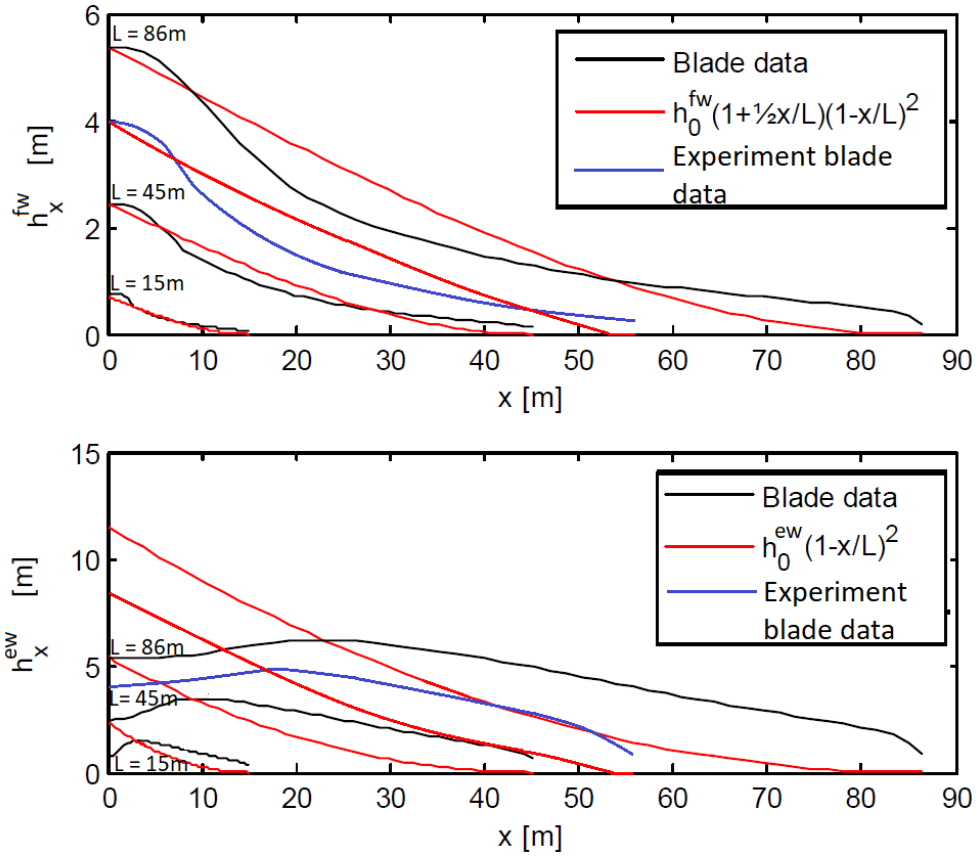

Figure 2.4: Typical blade geometries and the blade model the thesis will focus in compared with the respective strength-determined geometries [6].

It is important to observe that there are different data. They are from general WT blades geometries (marked with black), the experiment WT blade (marked with blue), and the results got from mathematical evaluations (in accordance with (2.18), (2.19), (2.20), (2.21)). The experiment blade data comes from Zhuzhou Times New Material Technology Co., Ltd. (株洲时代新材料科技股份有限公司) and is related to the blade model the thesis will focus on. The purpose of figure 2.4 is to show,

basing on stresses parameters on a WT blade, how the measures of h_x^{fw} and h_x^{ew} should be (according to the mathematical evaluations) and what they actually are (according to real features). As said before, the aim of this study is only letting the reader understand that measuring quantities like strain are essential to get a functional blade's model but are not enough to get it. In this case h_x^{fw} and h_x^{ew} are just simple parameters that will give a useless blade model if used alone; but are essential to get the result.

To have a clearer idea of what *flapwise* and *edgewise* mean, when represented on a WT blade, figure 2.5 could be illuminating. Moreover, as said in the previous pages, the *flapwise* deflection exists when a wind current (we are talking about a WT blade) hits a blade. The direction of the deflection will be the same (and exactly the opposite of the wind, once the blade turns back with its movement) of the current. The *edgewise* deflection is due to the gravity force. The deflection exists because of the rotation of the turbine: the faster the rotation is the more intense the deflection will be.

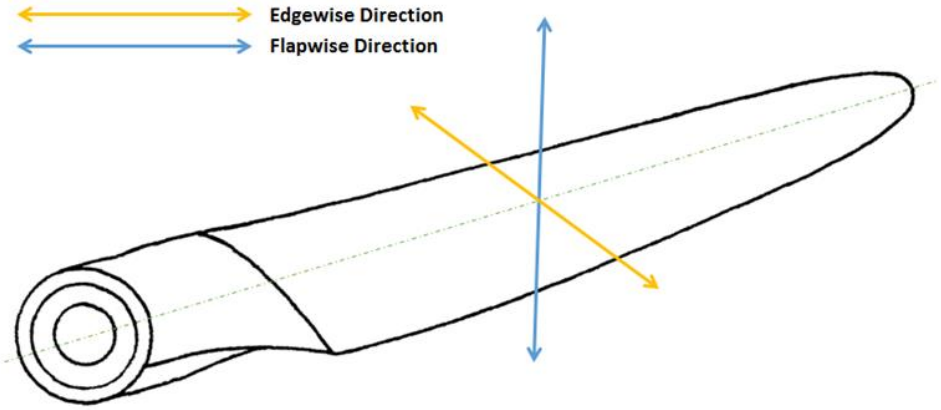

Figure 2.5: Representation of flapwise and edgewise direction of a WT blade.

2.4 - Stiffness of the blade

Stiffness is the rigidity of an object - the extent to which it resists deformation in response to an applied force [7]. To avoiding tower strikes by the WT blades, is important to analyse the blade's stiffness. The distance between the turbine and the tower should be enough long to prevent accidents. By using Bernoulli-Euler equations we can determine the transverse deflection, w:

$$\frac{d^2w}{\partial x^2} = \frac{M_x}{EI_x} \tag{2.22}$$

$$I_x = \frac{A^{fw}(h_x^{fw})^2}{2} \tag{2.23}$$

M_x is the moment of the beam at the general location x, E the material stiffness (known, as characteristic of the material), I moment of inertia. Solving (2.22) and (2.23), dividing the blade model into n parts, and considering $\theta_0 = w_0 = 0$, we can get the following equations:

$$\theta_i = \theta_{i-1} + \frac{1}{2}\left(\frac{M_i}{EI_i} + \frac{M_{i-1}}{EI_{i-1}}\right)(x_i - x_{i-1}); \quad i = 1, \dots, n \tag{2.24}$$

$$w_i = w_{i-1} + \frac{\theta_i + \theta_{i-1}}{2}(x_i - x_{i-1}); \qquad i = 1, \dots, n \tag{2.25}$$

Is then important to notice that E, the material stiffness, is relevant for the deflection calculation. If its value is high, the deflection should be shorter (actually the final value of the deflection depends on the product EI). Then, for an almost totally wood composed blade, the maximum accepted deflection would assume high values since the stiffness is usually low for wood; the highest value, 24.27 GPa, for "Massaranduba" wood, if compared to the value of a not so rigid material, like GFRP (whose stiffness is of 44 GPa), classifies wood as a not rigid material. Wood is present on the world with thousands typologies and surely their characteristics are different. However, the composition of wood is usually not uniform, that means a more precise study shall be done, but this is not the aim of this thesis.

Figure 2.6 represents the maximum deflection for blades made by different material (GFRP, CFRP, aluminium) as a function of the length and of the kind of design (fatigue or deflection).

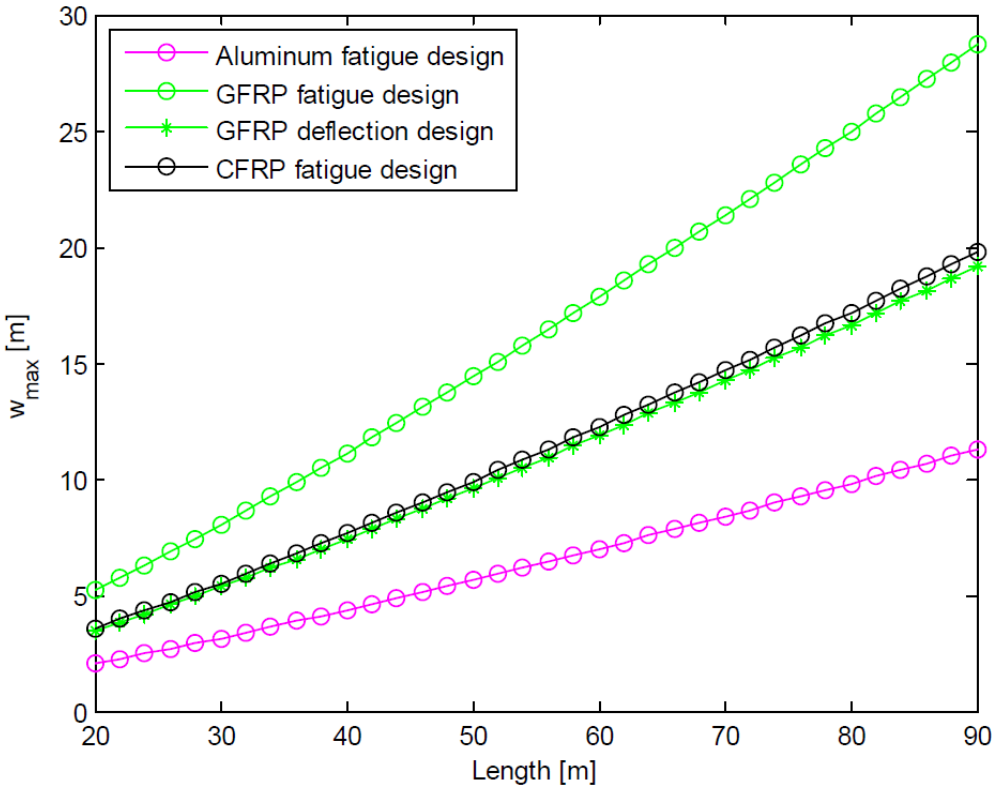

Figure 2.6: Deflection analysis as function of length and design of the blade [6].

2.5 - Weight distribution and deflection of the blade

The structure of the blade on which the thesis is focussing is special since wood, GFRP and an aluminium honeycomb core compose it. The aim of the thesis is describing different measuring instruments, which could measure strain on a WT blade. Since the structure of this blade is more complex than a normal GFRP one (for example), I will not examine it in depth. However, is important to have some blade weight predictions since we want to know how the blade is generally working. These evaluations will be useful for the development of the thesis.

GFRP, CFRP and aluminium will be considered as materials. Their physical characteristics are reported in table 2.1.

Material	Density, $[kg/m^3]$	Elastic modulus, $[GPa]$	Fatigue strength, $[MPa]$
GFRP	ρ = 1900	E = 44	σ_0 = 160
CFRP	ρ = 1600	E = 120	σ_0 = 300
Aluminium	ρ = 2700	E = 70	σ_0 = 100

Table 2.1: Mechanical parameters of the materials [6].

The weight predictions are function of the blade's length. Figure 2.7 represents a graph where the calculations have been done supposing the material has been loaded with the fatigue strength σ_0.

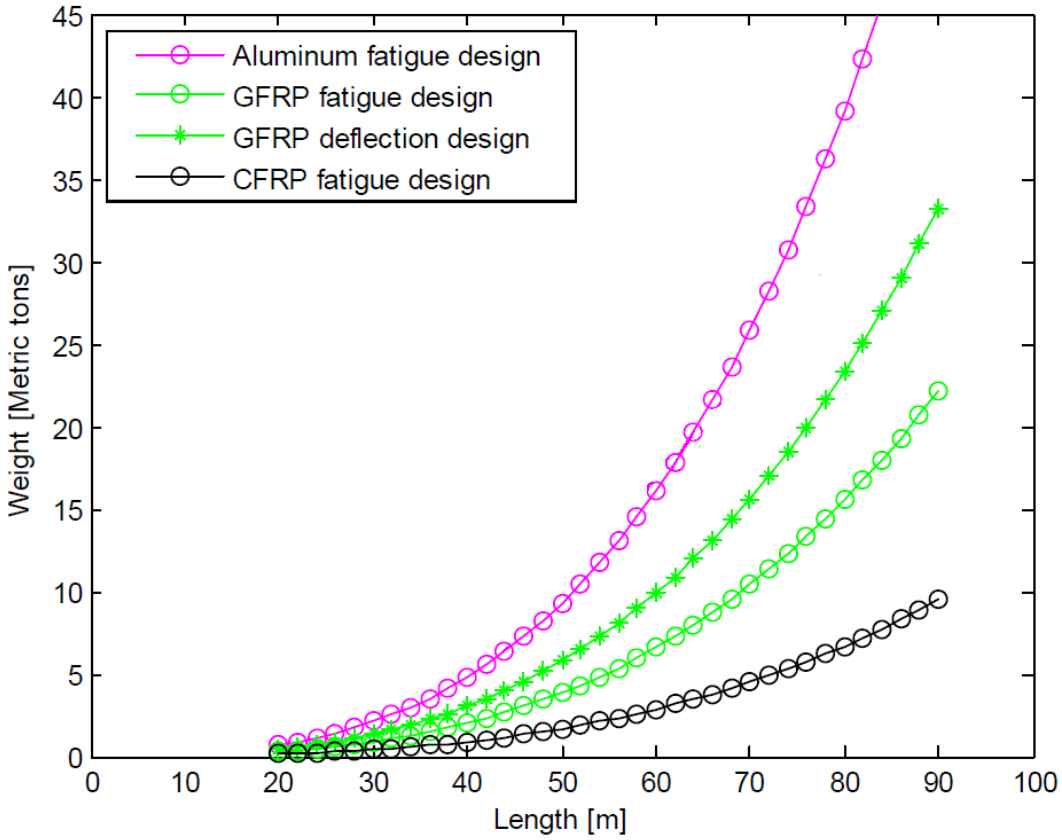

Figure 2.7: Weight predictions as function of the length of the blade [6].

Chapter 3

3 - Measuring instruments of mechanical parameters

Mechanical parameters are important factors in the field of the engineering (in the field of WT blades too). Measuring them before and during the mechanical component's life is essential to avoid eventual accidents (for example the wreckage of a blade). The responsibility is very high since the risk could bring to irreparable damages to the machine and to the safety of people.

The first strain measuring instruments were anaolg: they were objects like springs and levers. Originally not so much accurate, thanks to the help of Arnold Huggenberger, they have developed in accurancy and sensitivity. However, this kind of instrument has been overpassed by strain gauges since the results were more precise (even if the system was originally too expensive). Nowadays, resistive (strain) gauges are sensitive, accurate, easy to produce and they don't need big amount of material since it is used metal foil for the production. However, foil can only elongate so far, and this type of strain gauge does not work well for ductile materials. Conductive material can be added to elastomers for a stretchier gauge [8]. The result is a capacitive elastomer sensor. However, the strain gauges are not always a good compromise, particularly when the result must be an accurate and complete profile of a big mechanical component (like a plane or WT blade). In this case a big amount of gauges should be used (hundreds devices and hundreds wires). NASA introduced so FBG (Fiber Bragg Gratings). Fiber optic sensing is nowadays a well-known measuring system owing to its long lifecycle, wide operating temperature range, variety of measurable parameters; distributed sensing are preferable when compared to the strain gauge's ones. Moreover, the price of a common fiber optic sensor is becoming more and more competitive.

The instruments before cited are the most used. However, there are many other devices that can work and measure in this field. They are for example nanoparticle-based strain gauges (in this case the active area is made by conductive nanoparticles like gold or carbon), MEMS (microelectromechanical systems, that measure strains such as those induced by force, acceleration, pressure or sound), and vibrating wires (the wire is vibrating and the strain is measured by analysing the resonant frequency of the wire) [9].

3.1 – Strain: the basics

Strain is a measurement of deformation representing the displacement of particles in the body of a general object, relative to a reference length (the original length of the body).

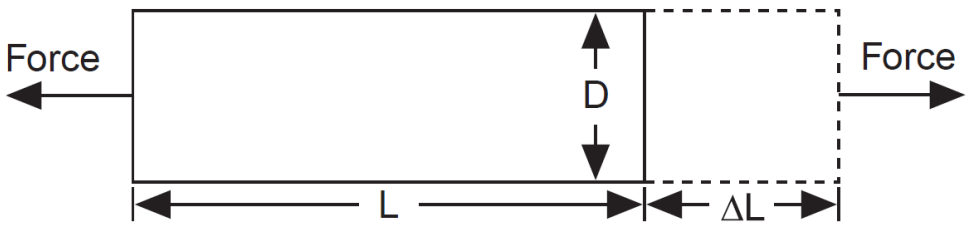

Figure 3.1: Strain definition.

Referring to what is represented in figure 3.1, the strain is defined as:

$$\varepsilon = \Delta L/L \tag{3.1}$$

When the material is tense, the strain is positive; when the material is compressed the strain is negative. The strain is usually small, particularly when we are measuring a mechanical component's stress. It's usually measured in $\mu\varepsilon$, microstrain.

Is important then to introduce ν = Poisson's Ratio, that is a coefficient related to the Poisson Strain, an event that causes the enlargement or restriction of the girth of a bar, once it's strained with an uniaxial force. Is true that:

$$\nu = -\varepsilon_t/\varepsilon \tag{3.2}$$

ε_t is the strain in the perpendicular direction.

3.2 - Strain gauges

Strain gauges are electrical measuring sensors. Their peculiar characteristic is that their electrical resistance changes when the strain of the material where they are located varies. The most used strain gauge is the bonded metallic gauge.

The gauge is usually composed by a grid pattern. In this way, the quantity of metallic material is arranged on the best shape in order to endorse the measurement of the strain and reduce the effect of the Poisson Strain that could threaten the results (to avoid the conditioning of the results by the shear strain and Poisson strain the cross area of the grid is minimized). In figure 3.2 is represented an example.

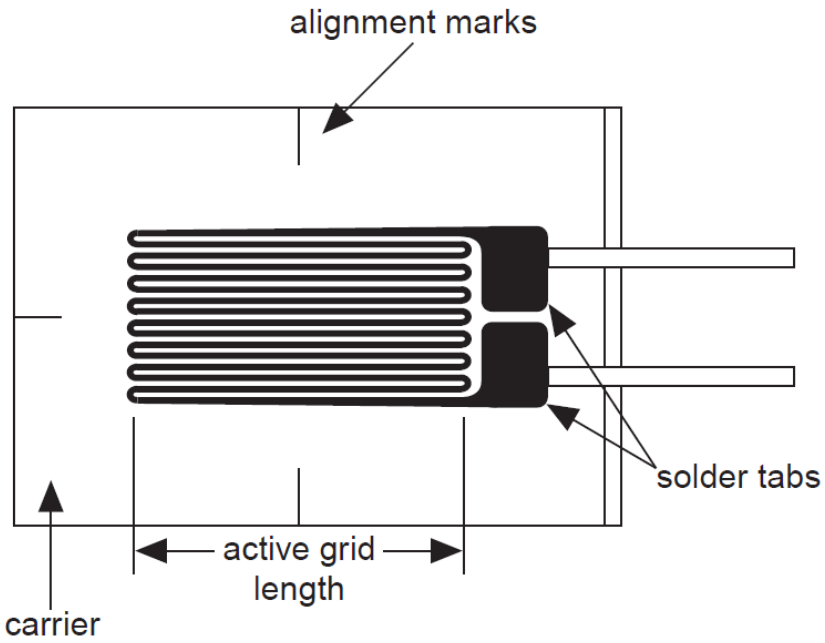

Figure 3.2: Bonded metallic strain gauge structure.

An important parameter is GF (gauge factor). It is defined as:

$$GF = \frac{\Delta R/R}{\varepsilon} \tag{3.3}$$

R is the gauge electrical resistance. $\Delta R/R$ is then defined as fractional change in electrical resistance. The gauge is not only sensitive to strain, but also to the temperature. Once the temperature has changed, there will be a material expansion or contraction (is obvious that this will bother the gauge during its job). The manufacturer tend to solve the problem compensating the gauge, but the sensitivity cannot be entirely deleted.

Being usually true that $GF = 2$, and that the strain usually assumes small values (rarely larger than few $m\varepsilon$) the fractional change in electrical resistance will be really small. This makes the measurement hard to take. To measure such small changes in resistance, and to compensate for the temperature sensitivity (as discussed in the previous section), strain gauges are usually used in a bridge configuration with a voltage or current excitation source [10]. This is the case of the Wheatstone bridge, as it can be seen in figure 3.3.

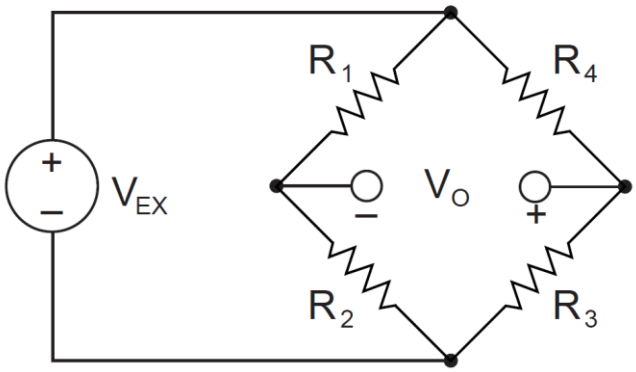

Figure 3.3: Wheatstone Bridge scheme.

In this case, V_{EX} is the excitation voltage. Applying then some electrical engineering principles:

$$V_0 = V_{EX}\left(\frac{R_3}{R_3 + R_4} + \frac{R_2}{R_2 + R_1}\right) \tag{3.4}$$

From (3.4), is evident that when $\frac{R_1}{R_2} = \frac{R_4}{R_3}$, $V_0 = 0$. Under these conditions, the bridge is said to be balanced.

Replacing, for example, R_4 with $R_G + \Delta R$, where R_G is the strain gauge resistance, and assuming that $R_1 = R_2$ and $R_G = R_3$, is true that:

$$\frac{V_0}{V_{EX}} = -\frac{GF\varepsilon}{4}\left(\frac{1}{1 + GF\varepsilon/2}\right) \tag{3.5}$$

The presence of GF in (3.5) entails a non-linearity of the system (respect to the strain), but the strain ε can be found. In this case, R_4 has been replaced by an active strain gauge; this means that any changes of the strain on the material (and then on the gauge) will cause a variation on the resistance and so the output voltage will never be null.

The sensitivity to the temperature can be minimized by using two strain gauges. One of them is active, while the other one (placed perpendicularly to the other one) is "dummy" (it can only measure the temperature, because the strain has negligible effect). In figure 3.4, is represented their disposition. Since the temperature measured by the two gauges is the same, the sensitivity to the temperature is minimized.

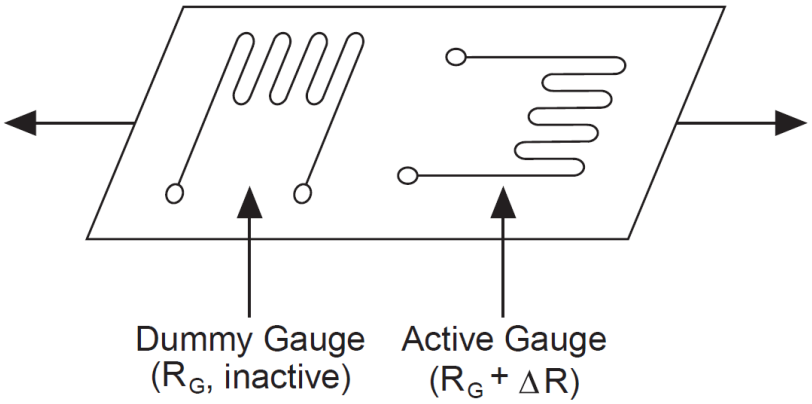

Figure 3.4: Eliminating temperature effects by using two gauges.

To achieve better accuracy results, two active gauges should be used, but in different directions. When a gauge is in tension its electrical characteristic is $R_G + \Delta R$, when in compression it will be $R_G - \Delta R$. The half-bridge configuration is exactly obtained using two active gauges: the main advantage is that the measurement will be more accurate since the precision is doubled.

By the way, the most complex but effective configuration is the full-bridge configuration (figure 3.5). The precision is maximized even though the number of gauges is bigger (there is a gauge in every arm of the circuit). The cost will be higher then.

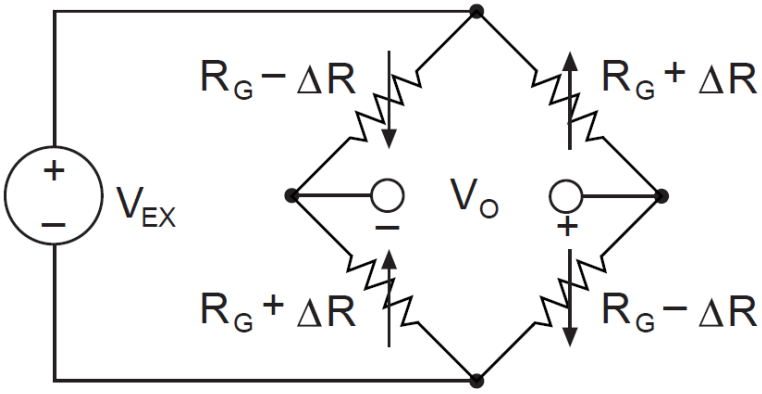

Figure 3.5: Full-bridge configuration.

The electrical output characteristic is described, for half-bridge and full-bridge configuration, as in (3.6) and (3.7). Is evident that the precision of the full-bridge configuration is double of the half-bridge's one.

$$\frac{V_0}{V_{EX}} = -\frac{GF\varepsilon}{2} \tag{3.6}$$

$$\frac{V_0}{V_{EX}} = -GF\varepsilon \tag{3.7}$$

In theory, the voltage output should be null as long as there is no strain in the component. However, resistances tolerances and strain induced by the application of the gauge cause an initial offset. There are two ways to correct it:

- Using a balancing circuit that can adjust the Wheatstone bridge and rebalance the total circuit, reaching a null initial offset.
- Compensating the initial offset with a software.

Strain gauges have discrete characteristics of sensitivity, accuracy, installation, and price. However, when compared to other technologies, they present some problems:

- Electromagnetic interference (EMC).
- Sensibility for the high explosive atmospheres.
- Possible mechanical failure of the material when exposed to high-level vibration loads.
- Requirement of big quantity of wires, since every sensor needs a cable (this comports also to a not negligible weight and high price).

3.3 - Optical fibre sensors

A major analysis of OFSs (optical fibre sensors) will be conducted later, since it is the base of the thesis. In this paragraph, some general features will be reported so that a comparison with the strain gauges and wireless sensors could be made.

The invention of laser inspired the research on fiber optics for communications, sensing, and other fields. This is because laser systems are able to send a big amount of data when compared to microwave or other electrical systems. The possibility to carry big amounts of data at fast speed, increased the attention on optical fibers. The development of optical fiber systems led to the production of several structures. An example is combining some products of fiber optic telecommunications field with optoelectronic devices field: the result is OFSs. Soon it was discovered that, with material loss almost disappearing, and the sensitivity for detection of the losses increasing, one could sense changes in phase, intensity, and wavelength from outside perturbations on the fiber itself. Hence, fiber optic sensing was born [11].

OFSs are nowadays spreadly used for measurement of physical properties such as strain (static and dynamic), displacement, temperature, pressure and SHM (Structural Health Monitoring). For example, the technology is used for:

- WT and plane's blades: flapwise and edgewise mechanical stress, pressure on blade's surfaces.
- Buildings, bridges: concrete/crack/prestressing/longterm deformation (creep and shrinkage) monitoring, spatial displacement measurement, concrete-steel interaction, and post-seismic damage evaluation [12].
- Tunnels: joints and convergence detection, prefabricated vaults evaluation.
- Dams: foundation/joint expansion/temperature monitoring, special displacement measurement.
- Mechanical components (cars, alternators…): temperature/stress/strain monitoring.
- Heritage structures: displacement/restoration monitoring, crack opening analysis, post-seismic damage evaluation [12].

OFSs reached a good position on the sensors market. The price is becoming more and cheaper and they have suitable characteristics:

- Small size and easy integration.
- Incapability of conducting electrical currents.
- Immunity to radio frequency/electromagnetic interference.
- Lightweight.
- Capability of sensing more quantities, like strain, pressure, temperature, acoustic signals.
- Ability to form sensing networks.

3.4 - Wireless sensors for wind turbine structural health monitoring

Being the main topic of this thesis the measurement of strain for a WT blade, it is opportune to introduce, as last example, the technology of wireless sensors. An increasing method to obtain a WT blade monitoring is using NDT (Non Destructive Technique). The monitoring of mechanical parameters of the blade takes place before and during the functioning of the blade (SHM). The technology of wireless sensors is retained one of the most useful for this kind of application. The last years have brought different wireless technologies that can be used for structural damage detection, including RFID (radio-frequency identification), that has been proposed for a wireless damage detection platform in civil engineering application. RFID tag sensors provide identification data and monitor of physical parameters of tagged objects without having an active sensor in the tag circuitry [13].

As in figure 3.6, the system of a RFID wireless sensor could be composed by a RFID reader (an active read out device), and a RFID passive tag (which include the sensor and the integrate circuit) that are used with wireless identification with another tag attached.

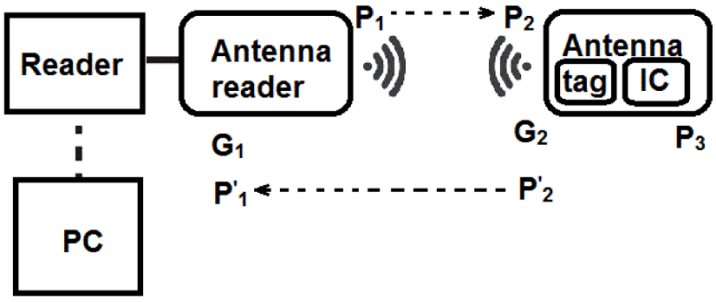

Figure 3.6: Wireless RFID sensor possible structure.

The structure has features so that a changing on dielectric property leads to a change in the resonance frequency displacement. The resonance frequency displacement varies in a linear way as long as the effort is small (typical for mechanical structures, including a WT blade). Two antennas are present, one for the reader (so for the sensor structure), one for the attached tag. Their working (interrogation) frequency is the same, so that it can be obtained a perfect matching between the antenna tag and the IC chip. A microcontroller then elaborates the information. The interrogation range is an important parameter for the sensor. The smallest power to activate the attached tag is obtained when the reader is working with the resonance power (necessarily).

The RFID typology of wireless sensor is not the only one. PWNS (Piezoceramic-based wireless sensor network system) was developed for automated real-time health monitoring of wind turbine blades in the work “Wind turbine blade health monitoring with piezoceramic-based wireless sensor network” [14].

As in the RFID technology, there are several advantages. For example, while the optical fibre sensor can only measure the strain in the place where it is located, the PWNS can measure it in a wider area and in real time (ideal situation for SHM). The proposed automated real-time piezoceramic-based WSN in [14] is composed by an embedded piezoceramic sensor and a wireless communication system. The embedded piezoceramic patch is utilized to create some guides to cover the whole blade. The waves are detected then from other sensors. The monitoring locations of the blade were chosen based on the physics of the blade (some parts are more stressed than others). The signals detected from the sensors are then transmitted by wireless to elaborators that will analyse the data. A scheme is represented in figure 3.7.

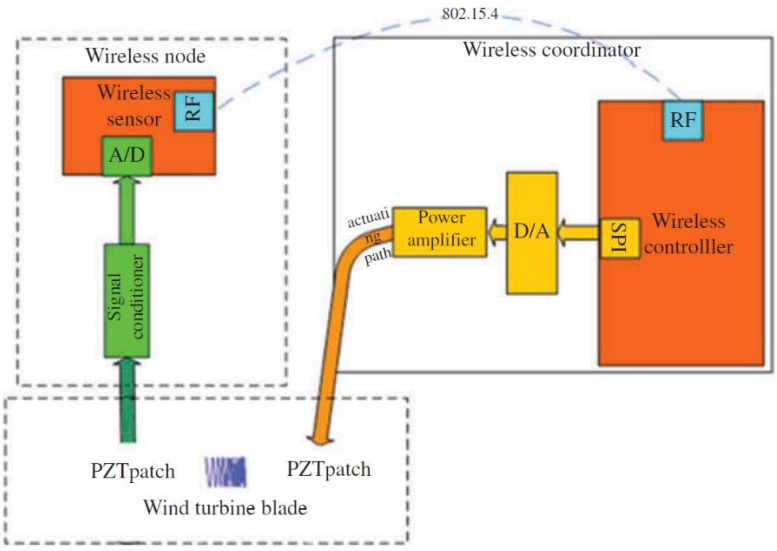

Figure 3.7: Block diagram of the wireless network [14].

WNS (wireless network system) is not only a strain and mechanical stress measuring system, but can measure other environmental parameters, like pollution index, temperature, sound, wind. WNS is a system composed by more sensors arranged in different places of the measuring environment; these devices are recording some specific physical conditions and sending by wireless connection to a data centre where the information will be collected and analysed.

The wireless sensors could be preferred to other sensors because:

- They can be used in hostile places, where wired systems (especially strain gauges, because they need big amounts of material, since the wires will be too many and too long, and the working conditions could be unbearable for them) could not be applied.
- They are scalable; in SHM, WNSs are then frequently used, since the information should be detailed, so more sensors should be used (using strain gauges will entail a large quantity of wires).
- They are easy to install.

On the other hand, they present some disadvantages. They have limited potentialities of communication, computation, battery power, storage.

Chapter 4

4 - Distributed optical fibre sensing technology

OFSs are devices using the light to transmit the information they are sensing. The typical structure of an OFS is illustrated in figure 4.1.

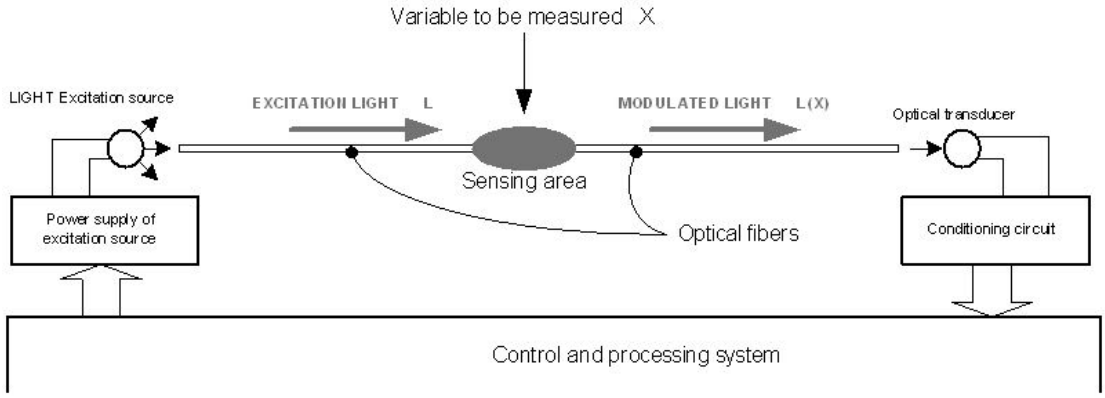

Figure 4.1: Typical arrangement of an OFS.

A power supply will provide the light excitation source that will probe the sensor. The optical fibre works as transit cable, conveying the light to the sensor and transmitting the modulated light to the optical transducer (in fact a patch panel) and interrogator then. This last one will convert the returned light into an electrical signal, in other words the output of the system.

4.1 - Distributed optical fibre sensors: a background

The DOFSs (Distributed optical fibre sensor) define the spatial distribution of a measurand[6] along the fibre. One of the advantages of the DOFSs is that the physical parameter will not be measured only in one location.

As for OFSs, the measurement is obtained by valuating parameters of the light like intensity, polarisation, phase, propagation time, optical spectrum and coherence [15].

The OFSs are separated into intrinsic and extrinsic category. In the first kind of sensors, the light stays within the fibre for all the length of the sensor. The modulation could happen by micro-bending, elongation (for example). In the second kind, there is an interruption along the fibre where a bulk-optic device will work as sensor. The second part of the fibre will collect the light emitted by the device, once the device itself has absorbed the light from the first part of the fibre and given off it with a different wavelength. Figure 4.2 could give a clearer view.

[6] The term "measurand" will be used in this thesis with the meaning of input of a sensor that will be converted into electrical or optical signal.

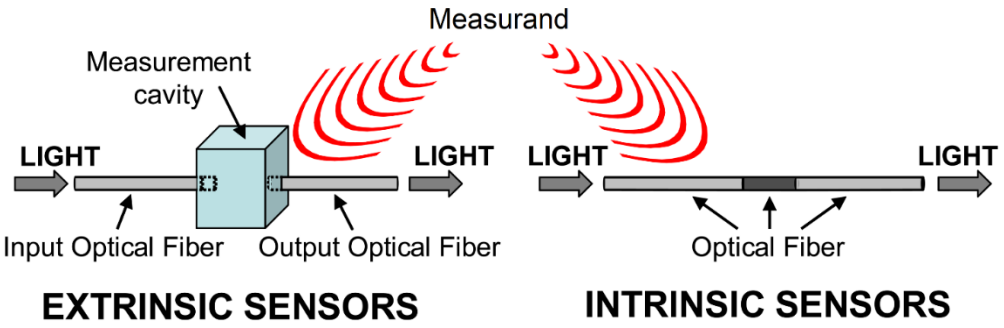

Figure 4.2: Representation of extrinsic and intrinsic OFSs.

Since the cost of technology has always been of primary importance in the engineering field, to achieve a good compromise in terms of cost-effective applications, multiplexed sensors have assumed a discrete prestige among OFSs. The technology consists of multiplexing several sensors onto a single fibre cable [16] and sharing the interrogator in different points. These devices gained acceptance, but they require complete and mapped spatial profile of the measurand, needing then a silly amount of sensing points (to complete the profile) or a prior knowledge of the distribution. This makes DOFSs the most effective multiplexed sensors, since they can measure a continuous spatial profile of the measurand along the entire sensing fibre. DOFSs are defined as intrinsic sensors able to define the spatial distribution of one or more measurands at each point along a sensing fibre [15].

The first DOFS was a temperature sensor, in 1982. It was demonstrated that a liquid-core fibre was sensitive to temperature when interrogated by OTDR (optical time domain reflectometry). However, the liquid-core fibre was difficulty deployable; the research brought to different technologies until when inelastic scattering made DOFSs available [15].

4.2 - Elastic and inelastic scattering

When the medium (the optical fibre) is inhomogeneous, scattering occurs. Scattering may be elastic or inelastic on the basis of E_{ph}, the energy of the photons. If the energy is maintained, the scattering is elastic, if not, the scattering is inelastic. Three kinds of scattering will be considered: Rayleigh, Raman, and Brillouin. Rayleigh scattering occurs when the frequency of the scattered wave is the same of the incident wave (the scattering is elastic). The small-scale fluctuations of the refractive index that cause Rayleigh scattering are frozen in the glass and the elastic process does not involve their motion [15]. On the other hand, when the frequency of the scattered wave is not the same of the incident wave the scattering is inelastic. The heat in the material (fibre) is controlled by molecular and lattice vibrations, carried by phonons. When the vibration frequency is high (~10 THz) it is Raman scattering; when the frequency is lower (~10-30 GHz) it is Brillouin scattering. In both cases, there is exchange of energy (from the medium to the light or vice versa). When the scattered light has lower frequency than the incident light, it means energy has gone, through phonons, from the light to the medium; the new spectral features are called Stokes lines. Vice versa, if the energy has gone from the medium to the light, the resulting light will emerge at higher frequency and will have features of anti-Stokes line. In Raman scattering phonons energy is related with unit thermal energy ($k_b T$, where the Boltzmann constant is k_b), therefore the anti-Stokes Raman process could give information about temperature. By the way, even if a longer discussion will take place in the next pages, Brillouin scattering is also sensitive to temperature (and strain). To get a clear view, figure 4.3 could be helpful.

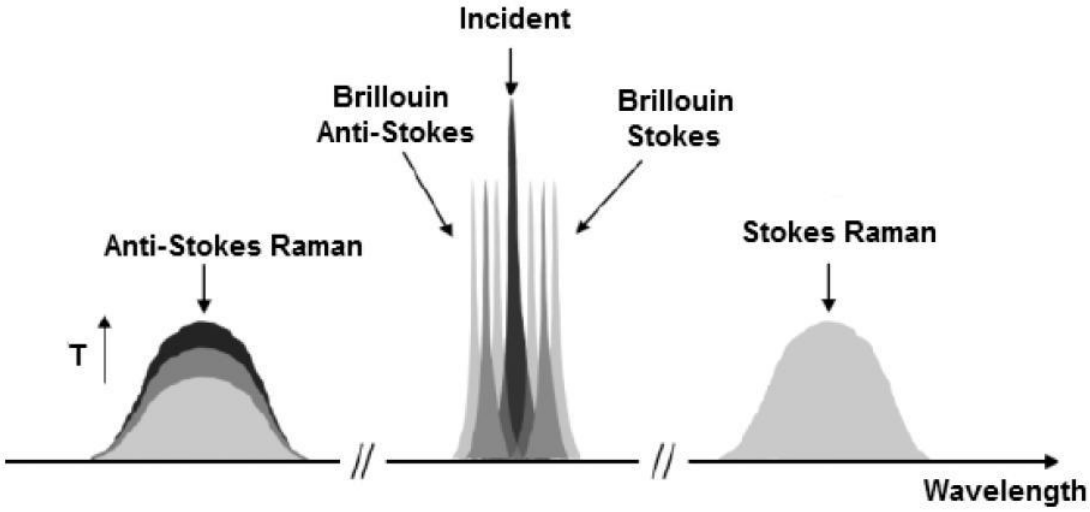

Figure 4.3: Raman and Brillouin spectra as function of anti-Stokes, and Stokes in standard optical fibres.

4.3 - Performance criteria in DOFSs

There are different parameters characterizing a DOFS; five criteria are going to be analysed in the following section.

The measurand resolution is the capability of the device to characterize tiny changes in the value of the measured quantity. For DOFSs, the measurand resolution is usually function of the position, since the light is more lessened when the distance from the starting point of the fibre is increasing.

The range is the maximum length that can be measured as sensing fibre (it is then important for determining the maximum pulse repetition rate, since the interrogator can launch the second pulse only once the first one has come back). The range is usually connected to the loss on the fibre since there is an acceptable limit of losses per unit of fibre. If the fibre is too long, the limit could be overpassed.

The spatial resolution is an important parameter that defines the ability of a DOFS to take measurements in closely spaced locations [15]. The spatial resolution is strictly connected to the measurand resolution. For example, even if the features of measurand resolution are finer than the spatial resolution's ones, being the result the convolution of the two factors, the measurand distribution will result attenuated.

The sampling resolution is the fibre distance between the samples that are present in the series of values given as output of the DOFS. The sampling resolution is related to the characteristics of speed of the light in the optical fibre and of sampling of the system. It should be finer than the spatial resolution in order to obtain a clear result (usually the sampling resolution is at least two times finer than the spatial resolution).

The measurement time is the time the system uses to get the results for all the points along the fibre, according to the requisites of measurand resolution.

Even if the criteria are concerning different quantities, they are all strictly connected by the signal-to-noise ratio. Being the signal in a DOFS usually small, the ratio will be small too; this limits the quality of the result. Then, to obtain a valid measurand resolution, a right way of cooperation between the parameters should be found.

4.4 - Propagation in optical fibres: physical concepts

An optical fibre is usually a long and cylindrical structure that guides the light. It is generally made by high-purity silicate glass. The structure contains a core, with refractive index n_1, a cladding, with refractive index n_2 (n_1 is usually higher than n_2, to let the light be trapped in the guide), and a polymer coating layer in order to protect the fibre. Introduced the Snell-Descartes law, (4.1), where n_1 is the refractive index of the medium from where the light is coming, θ_1 the angle from normal incidence, n_2 the index of the material of the medium where the light is going and θ_2 the respective angle, is true that:

$$n_1 \sin\theta_1 = n_2 \sin\theta_2 \tag{4.1}$$

An illustration can be found in figure 4.4.

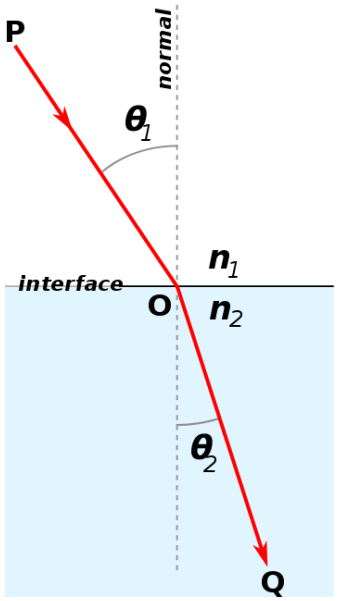

Figure 4.4: Representation of Snell-Descartes law of refraction.

If $\theta_2 = \pi/2$, the ray is refracted parallel to the interface; the critical angle is defined as $\theta_c = \sin^{-1}(n_2/n_1)$. Beyond this angle the light is completely reflected back; this condition is called "total internal reflection". Referring to the axis of the fibre, if the light is propagating at angles minor than $\theta_f = \pi/2 - \theta_c$, it keeps staying within the waveguide. NA (numerical aperture) is a term defining if a ray will be guided by the fibre or not.

NA is defined as:

$$NA = \sqrt{n_1^2 - n_2^2} \tag{4.2}$$

Since the topic is optical fibres, describing only a ray of light is too reductive. A plane wave with a specific wavelength and phase (spatially periodic) should be introduced. According to the electro-magnetic wave propagation, the wave can be described in terms of modes (this analysis would be more appropriate, according to the physics). Is then important introducing the factor V, the normalised frequency, defined as:

$$V = \frac{2\pi a NA}{\lambda} \tag{4.3}$$

a is defined as core radius, λ as wavelength. Fiber with a short radius and a small numerical aperture will then conduct only few modes (especially if the wavelength is high). Generally, in critical conditions (of radius and numerical aperture) the fibre will guide two modes, polarised orthogonally each other [15].

It is possible to distinguish some types of optical fibre.

The step-index multimode fibre is a fibre where the core diameter and numerical aperture are enough large to guide many modes. The boundary of the refractive index (between core and cladding) is marked (see figure 4.5). This limits the working conditions of a DOFS, since the output pulse will have an unclear profile.

The graded-index multimode fibre has been built to resolve the problems presented in the previous kind of fibre. In this case the index varies gradually from the core to the cladding (in this way in the area between core and cladding the refraction is attenuated). The radius is usually smaller than in a step-index multimode fibre. However, the properties of modes vary in a not predicted way in this case. Being the modes responsible of the transfer of power and so of the measurement result, this kind of fibre is still not completely satisfying.

The single-mode optical fibre has usually smaller core radius and numerical aperture than the previous ones, in according to let only the lowest order mode propagating. In this case $V = 2.405$ (the first zero of the Bessel function); the mode field pattern is a Bessel function (not a Gaussian, like in the previous cases, but similar). A representation of the different typologies of fibres is shown in figure 4.5.

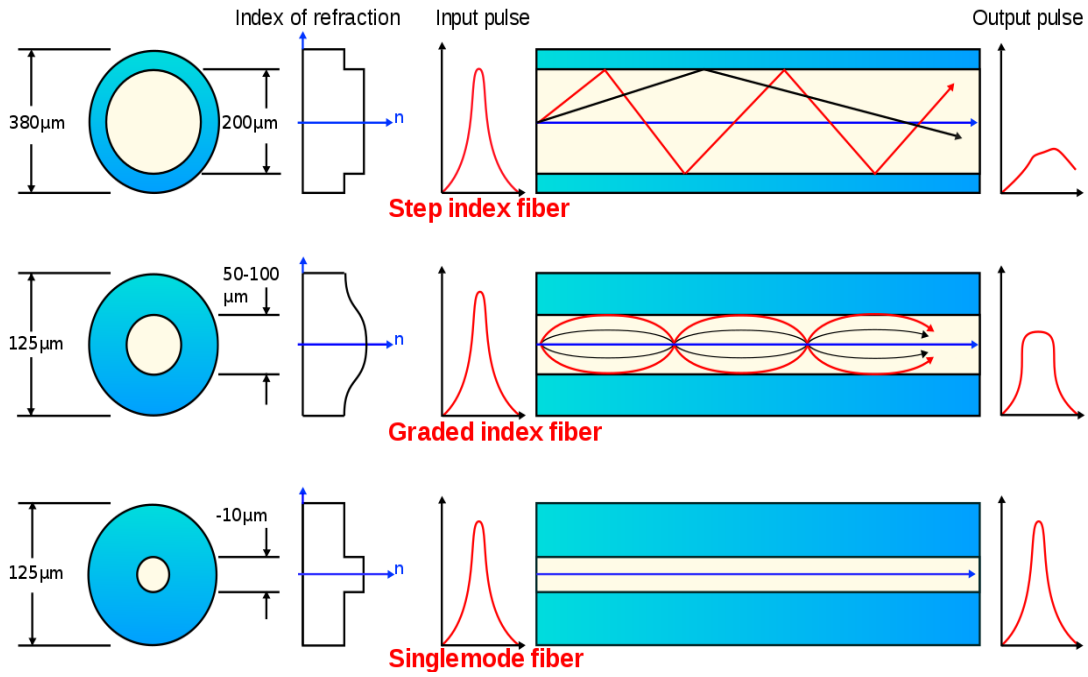

Figure 4.5: Representation of cross section, index profile, input-output pulse index of step-index multimode fibre, graded-index multimode fibre, and single-mode optical fibre (examples).

The losses in an optical fibre could occur mainly because of the absorption and of the scattering.

Modern optical fibres have already reached a good quality of manufacturing since the quantity of light they lose is small (a good fibre will only lose around the 20% of light in 5 km of length) [15]. The main loss parameters are:

- Silicate glasses present a low-loss transmission (related to electronic absorption) at short wavelengths (around 100 nm, the UV (ultraviolet) bands). For longer wavelengths (around 10 μm, the mid-infrared bands), the loss occurs by molecular absorption.
- Impurities like metallic ions and OH bonds are agent of absorption.
- Hydrogen can absorb light at high temperatures.

Scattering is a process where small amounts of physical quantities, such as light, sound, or moving particles, are deviating from their original trajectory by interactions with localized non-uniformities of the medium through which they are passing. The main agents of scattering, in the case of the OFSs, are:

- Rayleigh scattering, that occurs because of the thermodynamically carried fluctuations that happen on the medium. It is caused by inhomogeneities in the medium that are small compared with the wavelength of the light.
- Polarisation of the molecules through which the electrical field is passing (since the light is travelling through a dielectric medium). The effect of the polarisation is a phase delay.
- Mie scattering, an effect that occurs when the dimensions of the inhomogeneities are not small when compared to the wavelength.

In conclusion of this paragraph, is introduced the concept of bandwidth of an optical fibre. The bandwidth expresses the capability of an optical fibre to conduct information. The number of pulses that can be launched into an optical fibre is limited, since they become wider along the way. To define the pulse broadening the term “dispersion” is used. The bandwidth is inversely proportional to the length of the fibre; it is usually expressed as function of the distance. The term dispersion is broadly categorised as intermodal (i.e. differences of propagation time between modes) and intramodal (broadening specific to each mode) [17].

4.5 - Main components of a distributed sensing system

In a DOFS, more components are present to generate, guide, operate, and detect the light.

Lasers are important instruments for DOFSs, since they can generate a high power level light onto the optical fibre. Long fibres often characterize the DOFSs; the light has to be enough powerful to reach the end of the sensing system. A laser is composed by a gain medium (that amplifies the light) and a feedback that processes the light in order to obtain a stronger and more precise wave. More typologies of lasers exist:

- Broad contact semiconductor laser, composed by a semiconductor gain region (p-n junction) and a feedback part composed by faceting of a laser chip. This kind of laser is characterized by a high peak power and a poor quality spectral purity.
- Fabry-Pérot single-mode laser diodes launch a single transverse mode, but with lower power (to obtain a finer wave the facets of the feedback can support less power than the ones of a Broad contact semiconductor laser).
- Semiconductor distributed feedback lasers, which use the technique of Bragg reflectors creating some ridges in the gain region and obtaining a restricted band wave that will then be provided to the feedback.

Optical amplifiers are used before the sensing fibres and the detector (respectively when the signal is going to be launched and returning from the sensor point) to amplify the signal. Their characterisation is based on the gain and power they can supply. However, during the operation they always need to affront an obstacle; ASEs (amplified spontaneous emissions) and a noise background that accompany the gain signal provided.

Fused-taper couplers are used for connecting or splitting signals; the procedure consists on warming and stretching a number major or equal to two fibres touching each other. The result is a "mode sharing" by the new structure.

Isolators, circulators, Faraday rotation mirrors, are devices that respectively:

- Transmit light effectively on one direction, but block it when it comes from the opposite side.
- Transmit light from a first port to a second port and then transfer it to a third port (the light cannot go back to the first port once it has been transferred to the second port).
- Demodulate the light returning from the sensing fibre [18].

Modulators are useful devices that allow the frequency, intensity and direction of a laser beam to be modulated [19]. The existing technologies are AOM (acousto-optic modulators) and EOM (electro-optic modulators). The operation of an AOM is based on the interaction between an acoustic wave and the light wave (both travelling on the medium). On the other hand, EOM technology is also used for polarisation modulating.

Fibre switches are devices used to connect (in a discriminating way) a fibre to one of the possible output sets; if the system is complex (composed by many fibres), this operation is of fundamental importance. Fibre switches usually are MEMSs (micro-electro mechanical systems) if the switching time limitations are not too strict. They are transparent to the optical system.

Connectors and splices are instruments used to connect different sections of fibre, since for DOFSs usually the distances are long. There are different typologies of splices; it is preferable to use the fusion splice since the result will be more accurate, but if the condition does not let it possible, mechanical splice is available (easier application but less precise). On the other hand, connectors are used when the connection will not be stable (the sections will be more time connected and disconnected).

Detectors are used to transform the optical signal in electrical signal. Most frequently, an optical detector is composed by semiconductor photodiodes (PDs), which create an electron hole pair absorbing energy from the photons of light. The result is an electrical potential between the two parts of the device (electrical output).

4.6 - Optical Time-Domain Reflectometry

The technology of OTDR assumes a basic role in the field of the DOFSs. The OTDR technology was originally used for controlling the fibres in optical telecommunications (homogeneity, uniformity and attenuation of the light profile). A short pulse is launched in the fibre (with the help of an optical directional coupler); during the travel inside the fibre, the pulse loses a part of light because of the different phenomena discussed in previous sections (Rayleigh scattering is one of those). The scattered light is travelling in all the directions; then a part of it will fall within the angle of acceptance of the fibre in the opposite direction. The result is a return signal that also loses power during the travel. The return light is sent to a detector and elaborated. OTDR provides information on the continuity of a fibre; i.e. it informs the user of the existence and location of any break or high point-loss [15]. The reasons might be more: poor splice, bending of the fibre, connector broken, and fibre damaged. OTDR is a

helpful practice for DOFSs, since they usually use a long fibre. A scheme of an OTDR is represented in figure 4.6.

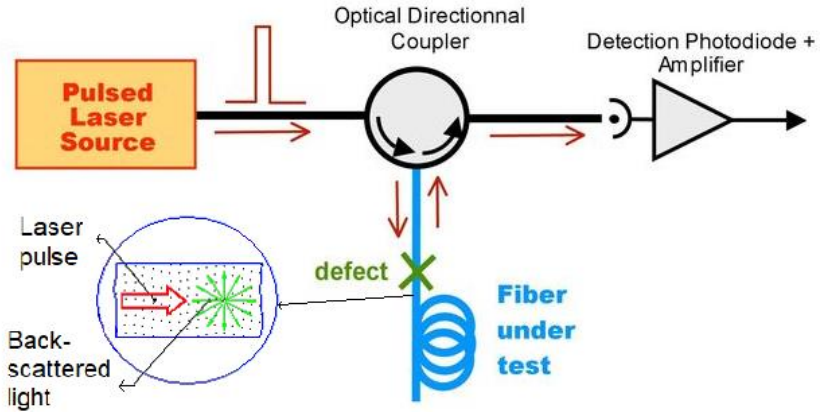

Figure 4.6: Schematic composition of OTDR.

Chapter 5

5 - Brillouin based distributed temperature and strain sensing

Brillouin scattering is a process that exists for optical fibres. As Raman scattering, which will not be deeply discussed in this thesis since it does not cover a primary position for it, Brillouin scattering is an inelastic scattering. It occurs with two supplementary frequencies on either side of the incident light. The frequency shift is ~10 GHz (while Raman's shift is ~13 THz) and the natural linewidth is ~30 MHz (while Raman's linewidth is ~6 THz) [15]. Is clear that in the field of measurements the quantitative characteristics of Brillouin scattering are preferable to the ones of Raman scattering (more explanations are going to be given).

The following considerations will focus also on Raman scattering even if the theory has not been discussed during the thesis. The aim is comparing it with Brillouin scattering.

While Raman "strain-dependent" frequency shift is only detected in crystalline (for example) [19], in Brillouin scattering the glasses themselves are responsive to strain and temperature in frequency and intensity. For Raman scattering, the natural linewidth is too large and is then not possible decoding the information brought by the crystalline part of the fibre. The same is not for Brillouin scattering, where the result is more precise since the whole fibre is bringing the information (in terms of scattering) and the linewidth is then briefer. Moreover, being the natural linewidth of Brillouin scattering not wide, techniques to improve the signal quality could be actuated (optical amplification…). The same cannot be said for Raman scattering, where the process is not working since the linewidth is too large.

In Brillouin scattering, the result is due to the cooperation of two counter-propagating waves: it is possible to let them interact in short distances having then spatial resolutions in the millimetre range [20].

Lastly, the spontaneous Brillouin backscatter signal is stronger than the Raman anti-Stokes backscatter.

5.1 - Spontaneous Brillouin scattering

SpBS (Spontaneous Brillouin Scattering) is an inelastic scattering that origins from the relation of the probe wave and the thermally driven material-density fluctuations (proceeding at the speed of the sound). During these interactions, a continuous exchange of phonons at different and many frequencies occurs between the wave and the material; this process changes constantly the refractive index through the stress-optical effect. The acoustic wave of the phonons produces a travelling fluctuation of the refractive index [21, 22]. On the other hand, Raman scattering occurs by movement of molecular vibrations; in the Brillouin case, the agents of the scattering are acoustic phonons, whereas in Raman case the agents are optical phonons.

Brillouin scattering exists with both longitudinal acoustic (LA, pressure waves) and transverse acoustic (TA, shear waves) [23]; actually, the LA are the real agents in the case of distributed sensing since the backscattered light of the TA is too weak and not able to bring enough information when the distance is long.

Is defined ν_B, the Brillouin LA lines frequency:

$$\nu_B = \frac{2n_1 \nu_0 V_A \sin(\theta/2)}{c} \tag{5.1}$$

ν_0 is the incident optical frequency, V_A acoustic velocity, θ the angle between the incident and scattered light, and c the speed of light in vacuum. Since all the parameters (except the incident optical frequency that is decided by the user) are function of the structure of the fibre, is possible to say that the frequency shift is also function of the material composition and the design of the fibre [24].

The spectral width of SpBS is function of the thermal phonons conditions, in terms of how long they can travel within the fibre before stopping. These conditions are in turn function of frequency (thermal phonons lifetime is strictly related to the frequency of the hypersonic[7] wave), and temperature of the fibre.

The Brillouin $\Delta\nu_B$ linewidth is defined as in (5.2):

$$\Delta\nu_B(NA) = \sqrt{\Delta\nu_B(0)^2 + {\nu_B}^2 \frac{NA^4}{4n_1^4}} \tag{5.2}$$

Generally, for silica, the material that is usually used to build an optical fibre, as the wavelength of the probe grows, the corresponding hypersonic frequency decreases. Moreover, the phonons resonance occurs in specific temperature conditions (to a certain temperature corresponds a specific energy, according to the thermodynamic physics). If the energy conditions let the resonance occurs, a high probe wavelength brings then a low hypersonic frequency. Being the absorption coefficient for thermal phonons proportional to the square of the hypersonic frequency (see (5.2)) [25], a high probe wavelength will bring a brief spectral width. In (5.2) is showed that the Brillouin linewidth is also dependent to the geometrical characteristics of the fibre (numerical aperture and reflective index of the core of the fibre). As the numerical aperture increases, the possible places (and angles) that the probe can hit are more; the scattered light will be stronger and the linewidth broader.

Even if in (5.2) only optical terms compare, the Brillouin scattering is also function of acoustic parameters. SpBS is result of the interaction between an optical wave and acoustic waves resulting from the backscattered light. As the optical waves are travelling in optical waveguides, the acoustic waves find in the optical fibre itself a contrast in acoustic speed: this means that the optical fibre is also an acoustic waveguide. The acoustic modes are important for the definition of the process; even if the waveguide is single-mode for the light, usually happens that exist more acoustic modes that define the result.

5.1.1 - Sensitivity to Temperature and Strain

As said in the previous sections, the frequency shift and the intensity of the spontaneous Brillouin backscatter are sensitive to temperature and strain [15]. The following formulas are expressed as in the refs. [26], [27] and [28].

$$\begin{bmatrix}\Delta\nu_B \\ \Delta I_B\end{bmatrix} = \begin{bmatrix}C_{\nu_B\varepsilon} & C_{\nu_B T} \\ C_{I_B\varepsilon} & C_{I_B T}\end{bmatrix}\begin{bmatrix}\Delta\varepsilon \\ \Delta T\end{bmatrix} \tag{5.3}$$

$$\begin{bmatrix}\Delta\varepsilon \\ \Delta T\end{bmatrix} = \frac{1}{\left|C_{\nu_B\varepsilon}C_{I_B T} - C_{I_B\varepsilon}C_{\nu_B T}\right|}\begin{bmatrix}C_{I_B T} & -C_{\nu_B T} \\ -C_{I_B\varepsilon} & C_{\nu_B\varepsilon}\end{bmatrix}\begin{bmatrix}\Delta\nu_B \\ \Delta I_B\end{bmatrix} \tag{5.4}$$

[7] Hypersonic and thermal assume the same meaning.

$$|\delta\varepsilon| = \frac{\left|C_{I_BT}\right||\delta\nu_B| + \left|C_{\nu_BT}\right||\delta I_B|}{\left|C_{\nu_B\varepsilon}C_{I_BT} - C_{I_B\varepsilon}C_{\nu_BT}\right|} \tag{5.5}$$

$$|\delta T| = \frac{\left|C_{I_B\varepsilon}\right||\delta\nu_B| + \left|C_{\nu_B\varepsilon}\right||\delta I_B|}{\left|C_{\nu_B\varepsilon}C_{I_BT} - C_{I_B\varepsilon}C_{\nu_BT}\right|} \tag{5.6}$$

The sensitivity coefficients of frequency shift $C_{\nu_B\varepsilon}$, C_{ν_BT}, and intensity $C_{I_B\varepsilon}$, and C_{I_BT} can be found by experimental way. Is noticeable from (5.4) (the formula is coming from the inversion of the matrix of (5.3), since its determinant is non-null) that the variations of strain and temperature ($\Delta\varepsilon$ and ΔT) are function of the frequency shift and intensity ($\Delta\nu_B$ and ΔI_B). For errors $\delta\nu_B$, δI_B the results in strain and temperature are as in (5.5), (5.6).

Typical values of the coefficients are as in (5.7), [26], [29]:

$$\begin{bmatrix} C_{\nu_B\varepsilon} & C_{\nu_BT} \\ C_{I_B\varepsilon} & C_{I_BT} \end{bmatrix} = \begin{bmatrix} 0.046MHz/\mu\varepsilon & 1.07MHz/K \\ -8\cdot10^{-4}\%/\mu\varepsilon & 0.36\%/K \end{bmatrix} \tag{5.7}$$

If compared to typical values of Raman scattering, it might be noticed that the responsiveness of intensity of temperature is lower for Brillouin scattering (i.e. $C_{I_BT} = 0.36\%/K$, while $C_{I_{R^8}T} = 0.8\%/K$, in the case of anti-Stokes line); this is actually a limit for Brillouin-based distributed sensor.

5.1.1.1 - Sensitivity of intensity to temperature and strain, and loss compensation for intensity measurements

The previous relations were relating the changes in strain and temperature to the frequency shift and the intensity simultaneously. However, it is possible to relate, for example, intensity to temperature and intensity to strain (separately). The two equations as in (5.8), (5.9), are from ref. [30].

$$I_{B_{as^9}}(T) = \frac{K_B}{\lambda_{as}^4}\left(\frac{1}{e^{\frac{h\cdot\nu_B}{k_B\cdot T}} - 1}\right) \tag{5.8}$$

$$I_{B_{s^{10}}}(T) = \frac{K_B{}^{11}}{\lambda_s^4}\left(\frac{1}{e^{\frac{h\cdot\nu_B}{k_B\cdot T}} - 1} + 1\right) \tag{5.9}$$

Is important to notice that as the temperature increases the intensity of Brillouin backscattered light tends to assume similar values for Stokes and anti-Stokes lines; this gives a limit to the system. On the other hand, for low values of temperature (few K), the result is different.

[8] "R" assumes the meaning of "Raman" in this case.
[9] "as" assumes the meaning of "anti-Stokes".
[10] "s" assumes the meaning of "Stokes".
[11] "K_B" is a term connected to Rayleigh scattering (no more explanations will be reported since this is not the aim of the thesis).

On the other hand, exists also a relation between intensity and strain (since K_B is function of temperature and strain). At temperatures lower than $\frac{k_B}{h} \cdot \nu_B$, the Brillouin intensity in one of the two lines normalised to the Rayleigh intensity is as in (5.10), from ref. [31].

$$\frac{I_B}{I_{R^{12}}}(T, \varepsilon) = \frac{T}{T_f} \frac{1}{E_\gamma \cdot B_T \cdot \frac{1 - \nu_p}{(1 + \nu_p) \cdot (1 - 2\nu_p)} \cdot (1 + 5.75\varepsilon) - 1} \tag{5.10}$$

(5.10) is a strain-temperature-intensity relation. Is important to define the following terms: E_γ, Young's modulus, B_T, isothermal compressibility, T_f, fictive temperature, and ν_p, Poisson's ratio [31].

Another useful parameter for Brillouin intensity measurement is defined as $\underline{LPR}$, that is the ratio of Rayleigh to Brillouin lines, in the spectrum of the light coming from the scattering. According to obtain an efficient measurement, the backscatter signal needs to be referred to another signal not responsive to the temperature. Since the Rayleigh line is near in frequency to the Brillouin line (the attenuation of the first one does not present a strong difference when compared to the second one), and it respects the previous requirement, the Rayleigh scattering shows up to be a good reference signal. The LPR is then related to the loss compensation for intensity measurements [15]. It is defined as in (5.11).

$$LPR(T) = \frac{I_R}{2I_B(T)} = \frac{T_f}{T} \frac{\rho V_A^2 B_T - 1}{2} \tag{5.11}$$

For glass, Rayleigh scattering's temperature is the fictive temperature (the temperature at which the inhomogeneities are fixed during the cooling process of the glass), whereas the Brillouin scattering temperature is the "real" temperature at which the measurement is occurring. LPR is in this case function of the temperature. However, for liquid materials the condition is different since the LPR does not relate to the temperature, but to the characteristics of the medium.

LPR finds an extended usage nowadays but has still some limits related to the strong noise of the Rayleigh scattered signal. Then, a large signal could be used to remedy the problem of the Rayleigh scattering, but on the same time, the signal would not be adapt for the Brillouin interrogation. The use of LPR as independent measurement technique of strain and temperature is rare, but it is usually used in multiplexed structures.

Since the problem of understanding if the quantity that is measured is strain or temperature has always affected the distributed sensors, LPR could be used as discriminator. As in (5.11), the definition of LPR is function of the intensity; then, having access to the intensity (and frequency-shift, eventually) data can help the user to understand if the measured quantity is strain or temperature (from a quantitative point of view, the strain and temperature related intensities assume different order values).

5.1.1.2 - Sensitivity of the frequency shift to temperature and strain

As seen in the previous part, strain and temperature are function of the intensity of the Brillouin scattering. The following part will describe the relation between frequency shift and the first two physical quantities.

[12] "R" in this case assumes the meaning of "Rayleigh".

As in (5.4), temperature and strain changes are function of the coefficients $C_{\nu_B\varepsilon}$, C_{ν_BT}: (5.12) is the relation between the quantities, as in ref. [32].

$$C_{\nu_B\varepsilon,T} = \frac{1}{n_{eff}}\frac{\partial n_{eff}}{\partial(\varepsilon,T)} + \frac{1}{V_A}\frac{\partial V_A}{\partial(\varepsilon,T)} \tag{5.12}$$

The responsiveness of the "total" refractive index n_{eff} to strain is function of the photo-elastic constants p_{11}, p_{12}, as in (5.13), ref. [15]:

$$\frac{1}{n_{eff}}\frac{\partial n_{eff}}{\partial \varepsilon} = -\frac{{n_{eff}}^2}{2}\left[p_{12} - \nu_p(p_{11} + p_{12})\right] \tag{5.13}$$

The main purpose in this case is calculating the coefficients $C_{\nu_B\varepsilon}$, C_{ν_BT} values. The optical fibres are only ideally made by pure silica. Actually, the composition varies fibre by fibre; is then hazardous using the previous formulas to get directly the values (since they are based on ideal conditions). The usual procedure to get the coefficients is taking a sample of optical fibre, strain it and measure its feedback. A comparison with the theory-based formulas (5.12) and (5.13) is finally done to prove that the results are truthful.

Is important to notice that all the considerations about the structure of the optical fibre reported in this thesis are ideal. However, in the reality the ideal situation is almost never respected. Moreover, the physical phenomena are described according to a simplistic theory.

Actually, the strain and the temperature propagate along the fibre in a complex and sometimes-unpredictable way. While the temperature and strain behaviour is usually static and predictable in the core of the fibre (the heat propagation from the top to bottom of the radius of the fibre core rarely spots strange tendencies), for the various coating levels of the fibre external part, it is not the same. Mechanical characteristics of the layers like Young's modulus and thermal expansion coefficient differ from the ones of the core of the fibre: this makes the measurement harder and more risky since the parameters of the coat vary the sensitivity of the system.

5.2 - Stimulated Brillouin Scattering

For the SpBS, a photon from the probe light is transformed into a scattered photon and a phonon. The group of scattered photons creates a backscattered wave. The direction could be towards the direction of the launched light or backward: as seen in the previous section the forward has almost null effect so the backward backscattered light has predominant importance.

When the power of the probe light reaches a determined level, the scattering starts to be stimulated; in other words, the pump power controls the process. Is important to notice that there are fixed power thresholds over which the effect loses its potentiality. The following considerations might be useful for a clear explanation of the phenomenon.

The electric field along the fibre might be seen as interaction of the optical waves traveling within the fibre. In the specific case of study, the modulated electric field moves at the same speed of the acoustic compressional wave (see figure 5.1). The main agent of SBS (Stimulated Brillouin Scattering) is the physical process of electrostriction, which provokes a change of some physical characteristics of the

[13] n_{eff} is used since the wave can travel in the covering and core of the fibre.

dielectric material when putted through an electric field. A change on the medium is also related to a change of the reflective index. The presence of a modulated electric field along the fibre finds an equivalent distribution of the reflective index: the result is a moving grating. Increasing the probe power influences the backscatter that in turn (according to the electric field principle described before) intensifies the reflection index. With an enough big gap between the power that is used and the threshold power, when the light power level is such that the relation between acoustic modes and reflection index withstands the scattering, the process is called SBS. A cycle has then taken shape: probe power-scattering-reflection index. An increasing probe power brings to an increasing scattering that in turn brings to a higher reflection index (see figure 5.1).

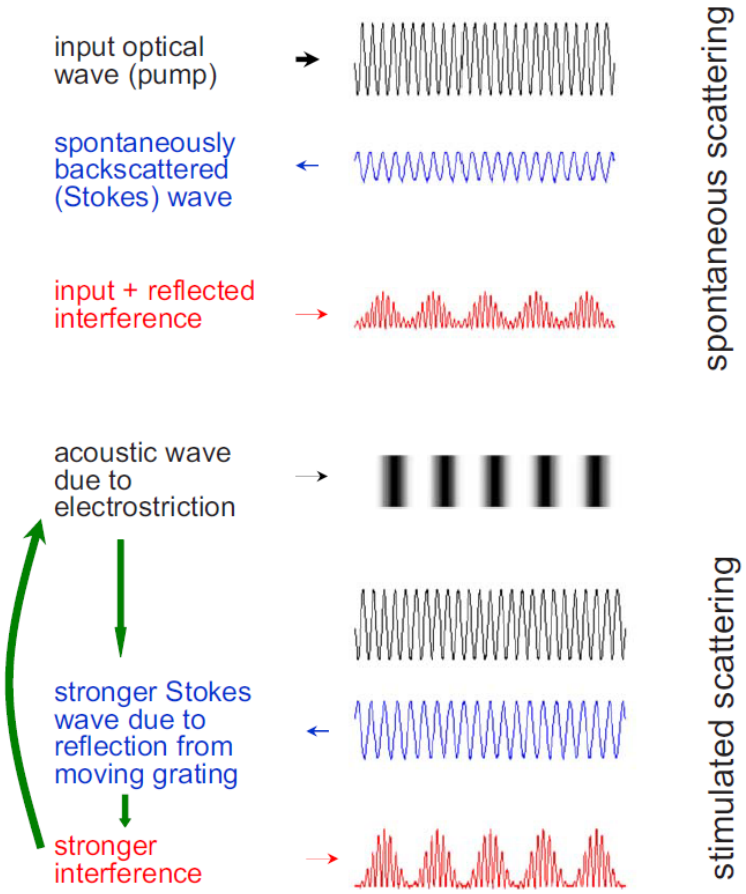

Figure 5.1: Different behaviours for SpBS and SBS.

It is important to take some remarks about the previous physical principle:

- In the previous considerations, it has been considered a single beam mode fibre.
- Acoustic modes assume fundamental importance for the SBS, and generally for the Brillouin scattering, since they amply the concept of optical fibre, which is in this case not only an optical waveguide but an acoustic waveguide too.
- As in figure 5.1, the acoustic wave (and so electrostriction) is the main responsible of SBS.

In the following equations (5.14) are reported the relations between the pump field E_p, the Stokes field E_s of the scattered or amplified wave, and the acoustic wave field E_a, as reported in ref. [33].

$$\begin{aligned}\frac{\partial E_p}{\partial z}-\frac{n_1}{c}\frac{\partial E_p}{\partial t}&=E_a E_s\\ \frac{\partial E_s}{\partial z}+\frac{n_1}{c}\frac{\partial E_s}{\partial t}&=E_a^* E_p\\ \frac{\partial E_a}{\partial z}+\Gamma_d E_a&=0.5\Gamma g_B E_p E_a^*\end{aligned} \tag{5.14}$$

Γ_d is defined damping factor; it is function of the phonons lifetime ($1/\Gamma_B$) and detuning factor $\delta\nu_B$ (the difference between the Brillouin shift and the actual value of the frequency difference between Stokes and pump wave). It is defined as $\Gamma_d = \Gamma_B + i2\pi\delta\nu_B$ [15]. On the other hand, g_B is defined Brillouin gain. The Brillouin gain might be seen as function (complex) of the angular frequency ω_s:

$$g_B(\omega_s) = \frac{g_B(0)}{1 - j2(\omega_p - \omega_s - 2\pi\Delta\nu_B)} \tag{5.15}$$

The real part of the function stands for the signal gain, the imaginary part for the variation of the reflective index. ω_s and ω_p are defined as angular frequency (variable), and pump angular frequency.

Finally, as in [34], might be interesting introducing the gain part $G_{SBS}(\delta f)$ (useful for a general sensor that uses SBS) of the transfer function $H_{SBS}(\delta f)$ of the Brillouin gain, considering the detuning factor $\delta f = \frac{\omega_p - \omega_s}{2\pi}$. Is then introduced (5.16).

$$\begin{aligned}H_{SBS}(\delta f) &= \exp\big(g_B(\delta f)\big) = \exp(G_{SBS}(\delta f) + j\phi_{SBS}(\delta f))\\ G_{SBS}(\delta f) &= \frac{g_B(0)\cdot {\Delta\nu_B}^2}{{\Delta\nu_B}^2 + 4\delta f^2}\end{aligned} \tag{5.16}$$

Chapter 6

6 - Description of the optical fibre sensing systems that will be used during the experiment

A more detailed description of the total sensing system will be found at Chapter 7. The measurement of the strain on the wind blade has been done using more sensing systems: FBG, BOTDA, and strain gauges. While the strain gauge operation has already been discussed, the aim of the following paragraphs is illustrating how the other optical fibre sensing systems are working.

6.1 - FBG

FBGs (Fiber Bragg Grating) are optical devices that present a periodic perturbation of the reflective index along the fibre stretch (fig. 6.1) [35].

The pattern is obtained by exposing the fibre core to an intense laser that modifies the properties of the fibre (when it is applied for a defined time). Hill et al. have demonstrated in 1978 at the Canadian Communications Research Centre (CRC), Ottawa, Ont., Canada, [36], [37], that putting a Germanium-doped fibre core through an Argon-ion laser will increase the reflection index until when the light is totally reflected. The increase of reflected light is related to the concept of "photosensitivity". The phenomenon consists of a coherent light travelling within the fibre, and meeting on the way a part of the reflected light. Interfering, they create a grating; the physical process occurs because the material is "photosensitive". If the agent of this is ultraviolet light, the grating is permanent. The magnitude of the index change (δn_0) is function of wavelength, intensity and duration of irradiation of the light.

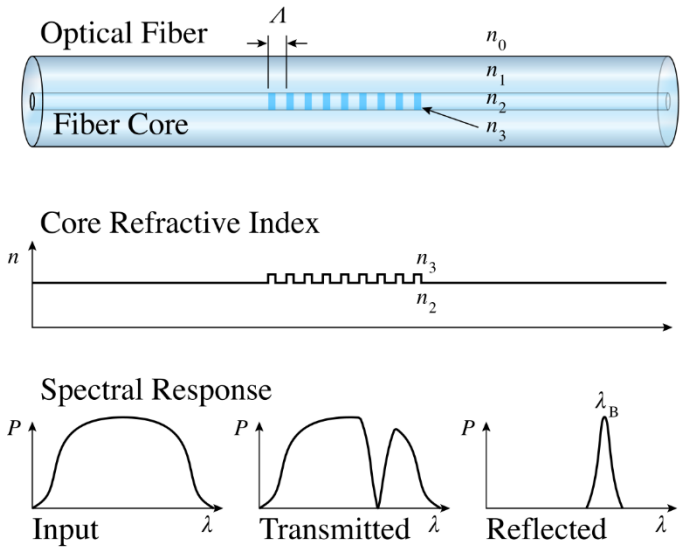

Figure 6.1: FBG physical structure, modal index profile, spectral description (input, transmission, and reflection).

Actually, the gratings might be seen as components of an optical filter since there is a part of light that is always reflected. The characteristics of the reflected light, especially its wavelength (λ_B, the Bragg wavelength), are function of the physical characteristics of the grating itself (see (6.1)).

$$\lambda_B = 2n_3\Lambda \tag{6.1}$$

As in fig. 6.1, n_3 is the modal index and Λ the grating period. All of the reflections are in phase. Since the changing of temperature and/or strain conditions causes a variation of the modal index and/or the grating period, FBG might be used also as fibre sensor (the Bragg wavelength will change too).

The grating features along the fibre might be seen as in (6.2).

$$\delta n(z) = \delta n_0(z)[1 + m\cos(2\pi z/\Lambda + \phi)] \tag{6.2}$$

The bandwidth is defined as in (6.3).

$$\Delta\lambda = \frac{2\delta n_0 \eta \lambda_B}{\pi} \tag{6.3}$$

δn_0 is defined as variation of mode index along the fibre (referring to fig 6.1, $\delta n_0 = n_3 - n_2$), and η is the part of power in the core.

The reflected power-peak is defined as in (6.4).

$$P_B(\lambda_B) = \tanh(N\,\eta(V)\delta n_0/n)^2 \tag{6.4}$$

N is the number of periodic gratings. $\Delta\lambda, P_B(\lambda_B)$ have been introduced since they result useful for having a clearer idea about fig. 6.2.

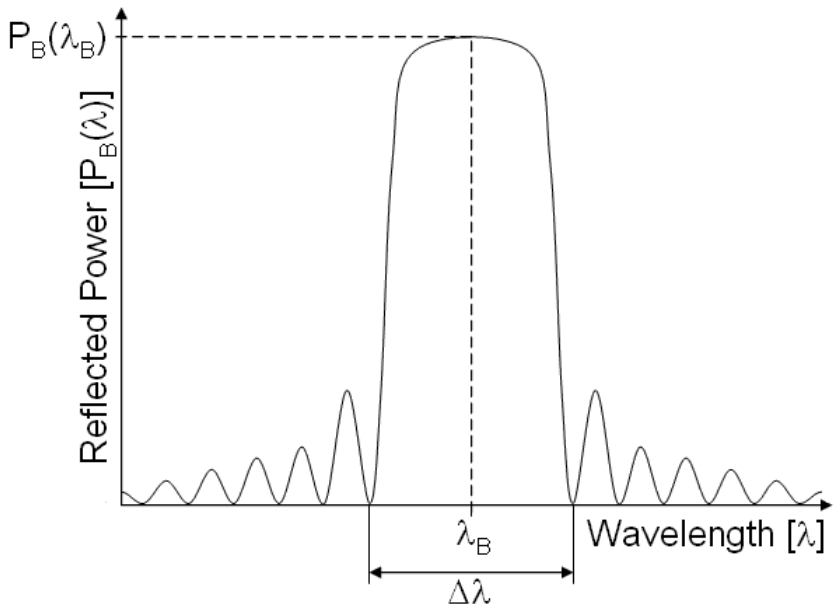

Figure 6.2: Graph of Reflected power/Wavelength.

FBGs find more applications in the field of the engineering. They are used for optical communications, as band-stop filter, in multiplexers and demultiplexers, since they can reflect with a narrow stop-band. They are used for optical sensing, since the Bragg wavelength is temperature and strain-sensitive. The changes in strain and/or temperature cause a Bragg wavelength shift ($\Delta\lambda_B$), as in (6.5), (6.6).

$$\frac{\Delta\lambda_B}{\lambda_B} = C_S\varepsilon + C_T\Delta T \tag{6.5}$$

$$\frac{\Delta\lambda_B}{\lambda_B} = (1 - p_e)\varepsilon + (\alpha_\Lambda + \alpha_n)\Delta T \tag{6.6}$$

C_S is the coefficient of strain, which is function of the strain optic coefficient p_e (comparing (6.5) and (6.6), is clear the relation). C_T is the coefficient of temperature, which is made up of the thermal expansion coefficient of the optical fiber, α_Λ, and the thermo-optic coefficient, α_n [38]. FBGs find application in seismology, pressure sensing (especially when the environment where they are going to be applied is extreme), and aerospace engineering. FBGs are also used as components of high power lasers, as high reflectors (HR) and output couplers (OC). They bring benefits since they eliminate the realignment during the life of the system. Finally, FBGs are used in double-clad fibers for matching active and passive parts.

6.2 - BOTDA

BOTDA (Brillouin Optical-Time Domain Analysis) is a system based on SBS. BOTDA uses two lights; they are emitted from two opposite ends of a single optical fibre. One of them is continuous, the other one is pulsed. As in ref. [15], on this elaborate the CW (continuous wave) will be called probe, while the pulsed wave will be called pump. A basic BOTDA arrangement is showed in fig. 6.3.

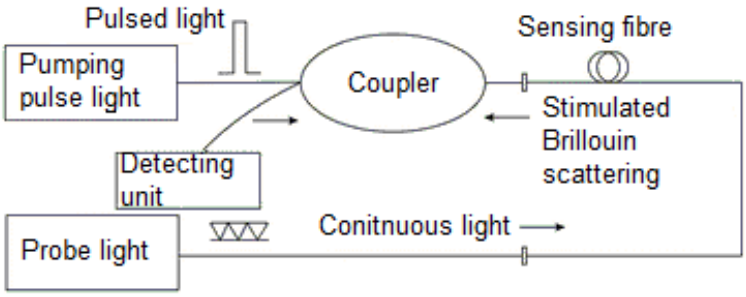

Figure 6.3: BOTDA standard arrangement.

The original function of BOTDA is defining the fibre attenuation, improving the technical capability of OTDR. The pump and probe signal are frequency-outdistanced of the Brillouin shift. Their interaction at the detecting unit-coupler is made up of a DC component that origins from the CW and is independent of position along the fibre, and a not DC component that is dependent of the position and comes from the interaction of probe and pump. (6.7) represents the not DC power value [39].

$$P_b^{\pm}(z) = \frac{g_B v_g}{2A_{eff}} E_p(0)\exp(-\alpha_p z)\, P_{cw}(L)\exp(-\alpha_{cw}L)\cdot \tag{6.7}$$

$$exp\left[\pm\frac{-g_B}{A_{eff}}P_{cw}(L)\exp(-\alpha_{cw}L)\frac{\exp(\alpha_{cw}z)-1}{\alpha_{cw}}\right]$$

$\pm$ is used because of the system characteristics; the probe is subject to the Brillouin scattering. Consequence is that the light will be amplified or attenuated. Then, the source applies directly to the probe an initial frequency of $f_{cw} = f_0 - v_B$, when there is amplification and $f_{cw} = f_0 + v_B$, when there is attenuation. $\pm$ is directly related to the formulas that have just been mentioned ("+" when there is attenuation, and "$-$ " when there is amplification). L is the length of the fibre, α_p and α_{cw} are the attenuation coefficients of the pulse and CW, A_{eff} is the effective area where the light is propagating, E_p the probe energy, and g_B the gain factor. The second part of (6.7), in other words the multiplicative component, might be omitted since it refers to the defects of the probe, which usually have not a strong impact with the final value (especially if the power is not high). Therefore, it can be noticed that the local variation power is only function of the pump, since the effect of the CW light is extended to all the fibre (all its length).

An interesting and basilar comparison with BOTDR might be done. The main difference between the two systems is that BOTDR is based on SpBS, while BOTDA is based on SBS. Actually, they are both working on the same interrogation domain, the time domain, but the presence of the CW light in BOTDA makes the biggest difference (easily predictably). It increases the signal level (depending on the value that the Brillouin shift assumes locally).

The relation between strain/temperature and Brillouin shift makes BOTDA a sensing system. Moreover, being the Brillouin shift function of the position (along the fiber length), BOTDA results a powerful measuring method that is able to output a detailed strain/temperature profile in function of the fibre length. However, the presence of CW entails the presence of a higher shot noise, but by using special techniques, good results may be reached. Moreover, as in BOTDR, it is required an enough big range that contains the Brillouin shift frequency, during all the measurement process. The conditions are function of the measurand and the fibre type.

Is important to take a note about the optical arrangements for BOTDA. One more difference between BOTDR and BOTDA is that for BOTDA the polarisation conditions of probe and pump affect the result in terms of loss or gain. In general is true that the Brillouin interaction is polarisation dependent; is then important adjusting the system in terms of operation. A rotatable half-wave plate is used to adjust the polarisation of the pump; the measurement is repeated with two orthogonal input states and the results are averaged [15]. In this way, the problem should be largely deleted.

6.2.1 - Sensitivity and spatial resolution for BOTDA

The concepts of sensitivity and spatial resolution are fundamental for a sensing system, since they are some of the main parameters that define its quality.

The resolution of the peak frequency (when the peak is a Lorentzian peak) is defined as in ref. [40].

$$\delta v_B = \frac{\Delta v_B + \Delta v_L}{\sqrt{2}SNR_e^{0.25}} \tag{6.8}$$

Usually, Δv_L, the laser linewidth, is negligible when compared to Δv_B. SNR_e is the ratio between electrical signal power and noise power. The modern technologies (that did not exist when the work of

ref. [40] has been written) brought developments to the quality of the laser. As result, the influence of Δv_L vanishes in (6.9), as in ref [41].

$$\delta v_B(z) = \frac{1}{SNR(z)} \sqrt{\frac{3\delta_{fs}\Delta v_B}{8\sqrt{2}\left(1-\frac{\delta_{fsu}}{\delta_{fs}}\right)^{1.5}}} \tag{6.9}$$

In (6.9) δ_{fsu} and δ_{fs} are the number of frequency steps sampling the Brillouin spectrum and the subset of those that are used in the fit [15]. Moreover, $SNR(z)$ is not related to the electrical signal. Therefore, in (6.9) the resolution is function of the position (since $SNR(z)$ is too).

As usually happens in engineering, the aim is finding the best trade-off among more parameters that characterize a technology. In the case of sensing, especially optical sensing, it is object of study finding the best compromise between the active (measuring) length of the fibre, the spatial resolution, the sensitivity of the system, and the measuring time.

Getting a reduction of pulse duration would increase the spatial resolution. Unfortunately, this technique has several disadvantages, since it would entail a reduction of the fibre part where pulse and Brillouin interact. The convolution of Brillouin linewidth and pulse linewidth makes up the gain spectrum; a decrease of the pulse duration will bring a broadened result (that results in a hard measuring local Brillouin frequency shift). In the standard BOTDA structure, the limitation is just below 1m, at an operating wavelength of 1550 nm in conventional single-mode fibre [15].

6.2.2 - Composite pulse techniques in BOTDA

The main interest of this paragraph is describing different techniques to achieve a good compromise between spatial resolution and system operation. The composite pulse methods for BOTDA are divided into single shaped pump interrogation, differential pump interrogation, and simultaneous gain/loss interrogation (all the methods that will be discussed in this paragraph are shown in fig. 6.4).

In the single shaped pump interrogation technique section, might be interesting have a first comparison between (a) and (b), fig. 6.4. As seen in 6.3.1, if the pulse duration is intensely lowed, the spectral width usually becomes wider. However, what has been observed in ref. [42] was that after having launched a series of short pulses, increasing the shortness would bring an unexpected result: the width would not broaden, but decrease. The spectral narrowing could be attributed to a poor extinction ratio of the modulator used in the experimental results [42]. The imperfect operation of the modulator activates a constant CW baseline that is always present, independently to the main pulse (it may be noticed the difference between (a) and (b), fig. 6.4). This brings to a constant optical-field that modifies the physical properties of the fibre, since the phonons are always ready to be probed by the main pulse. If the process works well the creation and the decay of the acoustic-wave do not exist; then the acoustic duration is enough long to ensure the not broadening of the Brillouin spectrum. The result is that the process is faster and the spatial resolution finer.

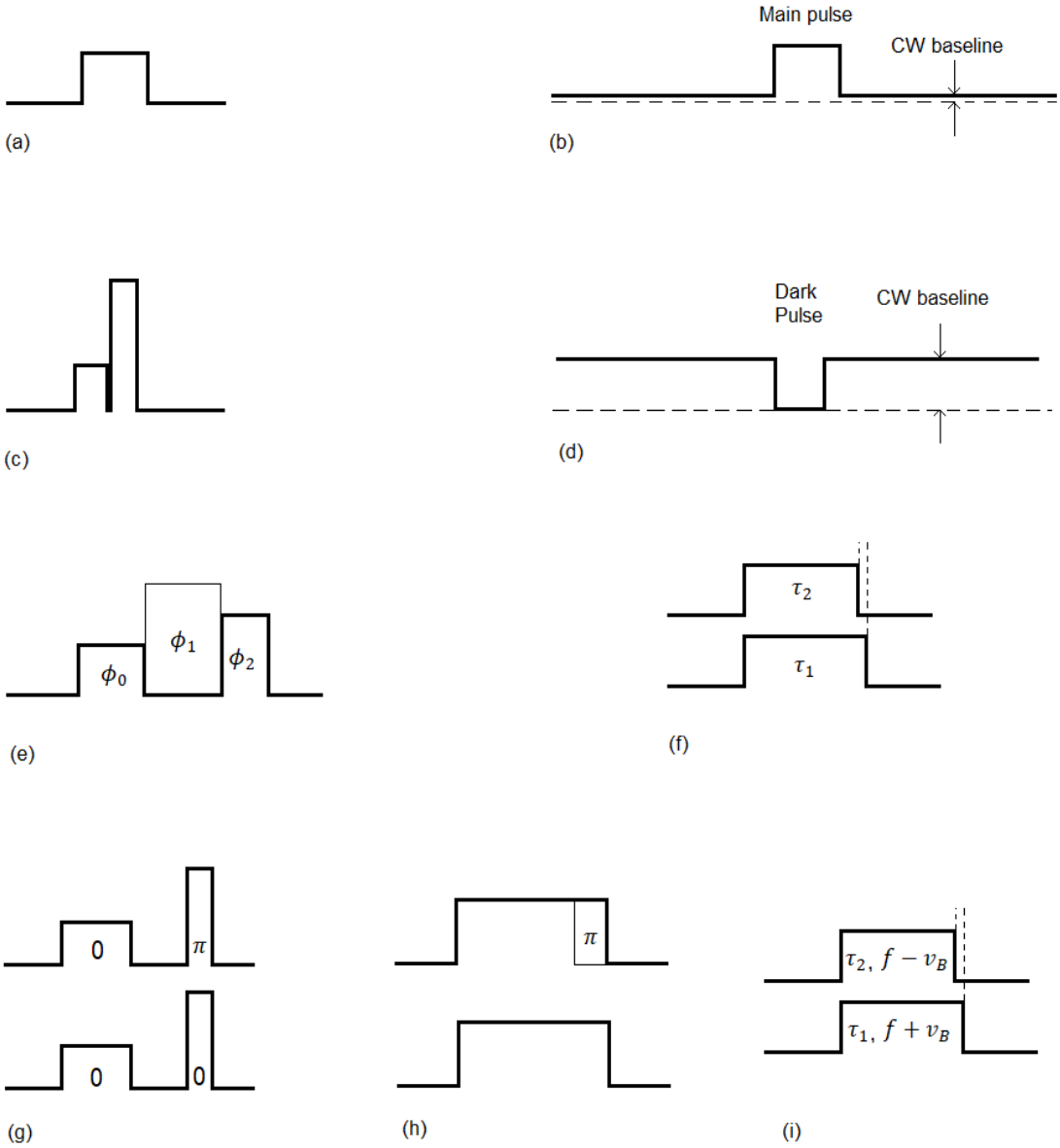

Figure 6.4: Some of the composite pulse techniques in BOTDA. (a) Single pulse; (b) single pulse with pedestal; (c) pump pre-pulse; (d) dark pulse; (e) generalised amplitude and phase coded pulse; (f) DPP-BOTDA; (g) negative Brillouin gain; (h) Brillouin echoes; (i) ODPA-BOTDA [15].

This concept has been used also for other methods. An example is (c), fig. 6.4. The first pulse is used to activate the acoustic-wave, while the second, stronger in intensity, assumes the role of the "main" pulse, interrogating the set wave. (d), fig. 6.4, represents the "dark-pulse" method: several intense short pulses are launched within the fibre. Since there is a strong link between the Brillouin scattering and the acoustic-field, the phonons result excited just where the Brillouin shift fits the frequency difference of the optical waves. If a dark pulse (a sudden and short break to the pulses) will be applied, the acoustic wave will be less affected (the phonons have a "long" life period, since they have been excited until the stop). On the other hand, the optical waves result more affected (decreasing and bringing then to a higher resolution). More generally, the technique might be used as arrangement of more pulses of different periods, as in (e), fig 6.4, or as unification of pre-pulse, dark-pulse and phase shifting, the three methods just analysed.

In the differential pump interrogation section, are used two pulses somewhat (lightly) different. The results are obtained by subtraction of the values of the unconnected acquisitions. As first method, (f), fig 6.4, two different duration signals are launched in succession within the fibre; it has been noticed that the spatial resolution is in agreement with the pulses duration difference (the smaller is the difference, the finer is the resolution). On the other hand, for DPP-BOTDA (differential pulse-width pair BOTDA) technique ((f), fig. 6.4), it is usually required a broad signal base; this entails a not accurate Brillouin profile acquisition (medium level distortion). The "negative Brillouin gain" technique, as in (g), fig. 6.4, is composed by two signals that are in turn composed by two pulses. The only difference between the two signals is the phase of the second pulse (is opposite to the phase of the second pulse of the first signal). The technique is still based on a first pulse that activate the phonons and a second pulse that interrogate them. The second pulse of the second series is not able to match the requirements for SBS, and then it interferes with the scattering provoked by the previous pulse; the result is a double effect. The "Brillouin echoes" method, (h), fig. 6.4, has the same working operation of "negative Brillouin gain" technique. These last two methods have the aim of fixing the distortion problems related to DPP-BOTDA.

In simultaneous gain/loss interrogation section, (i), fig. 6.4, might be an interesting example. Two pulses of lightly different duration are launched within the fibre, in the same time. One activates the Brillouin gain (anti-Stokes lines), while the other one activates the Brillouin loss (Stokes lines). Summing the two signals means operating a subtraction between two concordant signals that only vary lightly on duration. The requirements for obtaining a high resolution seem to be respected. The settings of this method are strict: the frequency of the two pulses must be symmetrically "distant" from the Brillouin shift frequency. Moreover, this has to occur precisely in every single point along the measurement part of the fibre; this means that the pulses frequencies requirements are local. A main difference between all the approaches that have been discussed in this paragraph is the domain. ODPA-BOTDA (optical-differential parametric amplification BOTDA), (i), fig. 6.4, works in the optical domain (instead of digital domain, as some of the other techniques previously discussed do).

Numerous scientists have achieved excellent results using the composite pulse techniques (in terms of spatial resolution, within the system operation limits). The techniques are efficient and the literature is keeping on working on new methods. However, other ways to improve the system potentialities might be followed.

6.2.3 - Pulse compression coding

In recent work of Bin Zan, Tsimuraya, and Horiguchi [43], pulse compression coding has been demonstrated as an extension of composite pulse methods. The technique is based on launching within the fibre a long pre-pulse and then a short succession of phase-coded pulses (within the phonons lifetime). After an enough long period (to permit the decay), another composite pulse is emitted. It is possible to define a relation between phonons lifetime and pulse generation: usually when the coded pulse duration exceeds the phonons population lifetime the system worsens. On the other hand, a set of coded pulses or a single pulse may be launched once the phonons have decayed (the phonons lifetime duration should be passed). The operation conditions in these two last cases are completely different but both of them are performance-improving criteria.

6.2.4 - Performance and limitations

A first limitation of BOTDA might be identified by the phenomenon of slow light. Given its very narrow gain spectrum, the gain or loss of Brillouin scattering is associated with a change in the group index through the Kramers-Kronig relations [15]. This means that a univocal relation between the spectrum and the group index does not exist. Therefore, the group index will change in according to the spectrum conditions. The consequences are:

- The expected location of the Brillouin shift cannot be identified.
- The time delay is different in the two cases (gain or loss); usually for the loss configuration, it assumes higher values (130ns in the worst case of a fibre having uniform loss spectrum along its length).
- The spatial resolution is also unpredictably changeable.

To overcome this problem a re-map in terms of distance along the axis in function of the slow light presence should be carried out.

A second limitation of BOTDA is the time required to take the measurement. Progresses have been done in terms of probe/pulse spectra. The main time-demanding factors are locating and determining the frequency offset (between the Brillouin shift and the pulse), and scrambling the polarisation. Therefore, repeated captures along the profile of the fibre are required. The strategy is measuring more than one frequency of the Brillouin spectrum at a time, with a set of several examining frequencies launched together.

Firstly, might be interesting focussing on the work that has been conducted in ref. [44], where a frequency comb replaced the probe. The process is faster since each of the frequencies launched in the comb can interact independently and concurrently with the pump. Moreover, it is not necessary determining systematically the relation between probe and pump, since the measurement is done in parallel by the comb (see fig. 6.5, (a)).

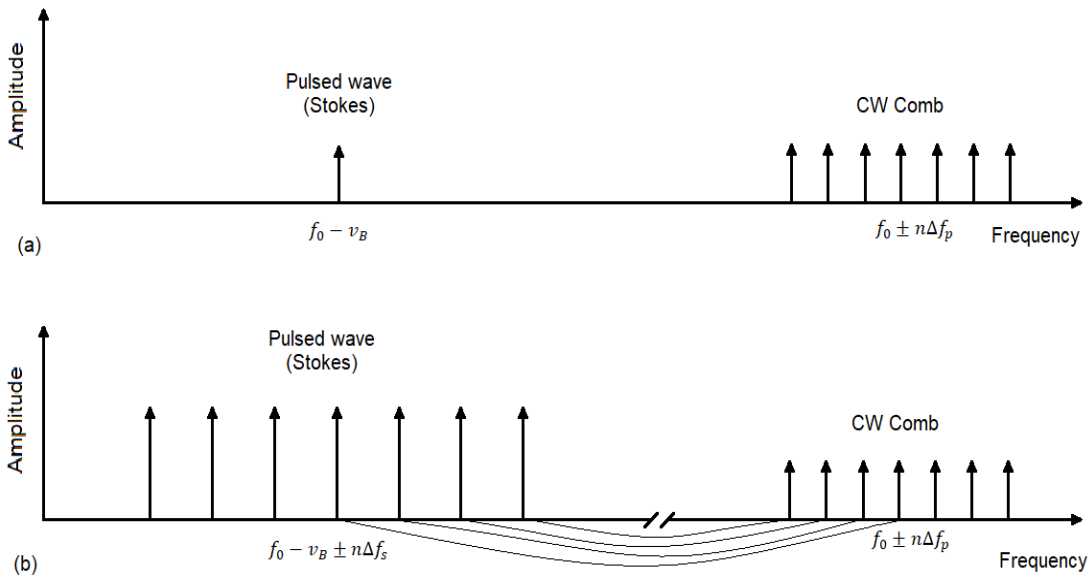

Figure 6.5: Parallel (multi-tone) acquisition: (a) Single comb [44], (b) Dual-comb [45].

However, some problems related to the signal processing were present; since the Δf_p should be enough short to have a good reconstruction of the scattering profile, and the signal processing needed to elaborate every single relation probe comb frequency-Brillouin scattering, the process resulted much time-costly.

By modifying the spectra of both probe and pulse, a development has been reached. What Voskoboinik et al. have done in ref. [45] has been creating two interacting comb series (for probe and pulse) with a lightly different comb spacing ($\Delta f_p \neq \Delta f_s$). As in fig. 6.5, (b), the technique SF-BOTDA (sweep-free BOTDA) sees each probe wave interacting with a different part of the Brillouin spectrum of its own pump; therefore, each probe/pump combination addresses one point on the Brillouin spectrum [15]. Since every line of the probe/pulse comb has an associated line of the pulse/probe, the system results much faster on the acquisition of the data.

A third limitation for BOTDA (it has already been partially discussed) is the distance. Even if BOTDA is usually characterized by a long achievable distance, sometimes it might not be enough. As it follows, a general length extension option has been found for optical amplification. For this distributed system, the signal should reach adequate power values (for both pump and probe). The power limitation is usually respected using more power modulators that in turn amplify (in moderation) the power along the fiber (instead of less modulators that inject higher-level power).

Lastly, the fourth limitation is the power itself. The reason is SPM (Self Phase Modulation): the phenomenon brings to a broadening of the spectrum. Moreover, the effect is gradual along the fiber. SPM is directly related to the time derivative of intensity; it means that short pulses will have a negative effect on the system. A solution is found in ref. [46], it is frequency-diversity, which is launching multiple interrogating signals at clear outdistanced frequencies. The non-linear effects are then partially deleted; to complete the improvement, a network of FBGs that cancels the time offset between BOTDA signals on their return from the fibre has been built up, as in ref. [46].

Chapter 7

7 - The experiment

The aim of this chapter is to introduce the total sensing system used during the experience and analyse the obtained results.

7.1 - The sensing system components

As said in the previous chapters, three sensing systems have been used. The need of three sensing systems is due to technical reasons, since the characteristics are different and there is need to compare them reciprocally; moreover, the systems can work complementary.

The used strain gauges are commercial products; their relevant specifications are listed in Table 7.1.

Reference temperature	23°C (73°F)
Maximum strain	3% or 30000 μS
Hysteresis	Negligible
Fatigue (at ±1500 μS)	> 10000000 cycles
Smallest bending radius	3 mm (1/8")

Table 7.1: Used strain gauges specifications.

Moreover, a set of FBG sensors has been used. The features in terms of wavelength of the FBG sensors are listed in Table 7.2. Except these parameters, which change from sensor to sensor, the other characteristics, which are the same for all the FBG sensors, are as it follows:

- Width: 0.2 nm.
- Reflection: 10 dB.
- SMSR: 15 dB.
- Pigtail: 3.0 m / 3.0 m.
- Stripping: 15 mm.

FBG set features	FBG 1 (CH1)	FBG 2 (CH1)	FBG 3 (CH1)
Wavelength (nm)	1.524,37988	1.535,29480	1.542,42228
	FBG 4 (CH1)	FBG 5 (CH1)	FBG 6 (CH1)
Wavelength (nm)	1.548,30980	1.554,45988	1.555,45756
	FBG A (CH2)	FBG B (CH3)	FBG C (CH4)
Wavelength (nm)	1.550,31396	1.549,90412	1.549,47043

Table 7.2: FBG set features.

For these sensors, the Micron Optics Dynamic Optical Sensing Interrogator (sm130-700) has been used. It has four optical channels, a scan frequency of 1 kHz, and a wavelength range of 1510-1590 nm. It is then clear why the distribution of the 9 FBGs represented in Table 7.2 has been done using 4 channels (FBG 4, FBG A, FBG B, FBG C have similar wavelengths, so it has been preferred to divide them into 4 different channels).

Lastly, a teflon-rubber coated standard single mode optical fibre has been used. The coating helped the laying of the fibre on the blade, since the required length was high, and a simple (not coated) optical fibre was easily breakable. A DiTeSt STA-200 Series (Omnisens®), based on the Brillouin scattering, has been used to interrogate the fibre itself. The features and performances of the interrogator are as following:

- Number of channels: two independent and selectable channels (standard).
- Sensor configuration: two fibers (loop) or single fiber (mirror-ended) configuration.
- Sensing fiber: standard single mode fibers.
- Distance range: 50 km.
- Spatial resolution: 0.5 to 20 m (by increment of 0.1 m), 1 m at 20 km / 2 m at 30 km / 3 m at 50 km.
- Distance resolution: 0.25 m.
- Number of distance points: 100000.
- Dynamic range: 10 dB (with no effect on performance), up to 20dB for distance up to 6 km, with 1 m spatial resolution.
- Measured variables: Strain, Brillouin Frequency shift, Brillouin gain and width.
- Acquisition time: > 10 seconds, 1-2 minutes typical, 5-10 minutes for high resolution.

For Brillouin frequency shift, temperature and strain, the parameters are as in Table 7.3.

	Brillouin Freq. Shift	Temperature	Strain
Resolution	0.1 MHz	0.1°C	2 μS
Range	10 GHz to 13 GHz	from -273°C to 700°C	from -3 % compression to 3 % elongation

Table7.3: DiTeSt STA-R Series working conditions.

7.2 - The object of the measurements

The object of the measurements is a wind turbine blade designed and fabricated by the company Zhuzhou Times New Material Technology Co., Ltd. (株洲时代新材料科技股份有限公司) that requires to be tested. Figure 7.1 is a representation of it.

Figure 7.1: The object of the measurements.

The length of the blade is around 60 m. It is composed by a main structure made of fibreglass (to maximize the ratio between resistance and weight). The other parts have to be introduced partially, according to the secret policy of the company.

The main framework is almost totally covered by wood, except the main beam, represented in figure 7.2.

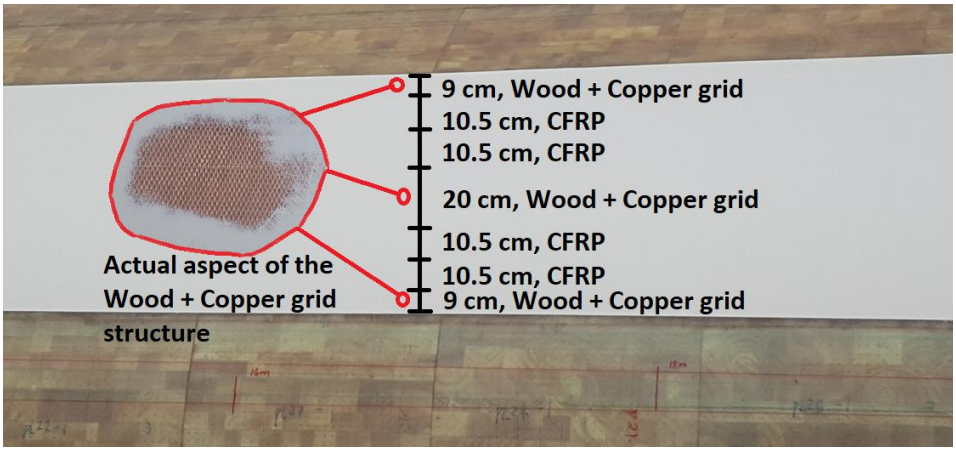

Figure 7.2: Structure of the main beam of the blade.

There are two lateral parts large 9 cm, and a central part large 20 cm, composed by a reticulated unit made of copper and wood (as in figure 7.2 - detail), and two other parts (that are in turn made up by other two subunits large 10.5 cm) made of CFRP (Carbon Fibre Reinforced Polymer). LE (Leading edge) and TE (Trailing edge) of the blade are made of GFRP (Glass Fibre Reinforced Polymer). The wood cover of the blade is composed by two kinds of material (see figure 7.3).

Figure 7.3: The border between the two kinds of wood that compose the blade cover.

The blade's structure is finally cover with a thin layer of fibreglass.

7.3 - The sensing setup

Strain electrical gauges compose the measuring system adopted by the company, while optical fibres (FBG, BOTDA) compose the measuring system adopted by us. The aim of the operation is integrating the two schemes to obtain a partial comparison and eventually ulterior values (in the case some sensors are not working, the complementary ones might give a value).

The requirement of the company is measuring determinate locations of the blade that have been identified naming them by some points. The electrical gauges setup covers all the points while the optical fibres setup covers a part of them. The reason is that the company gave to us a shorter period for the installation of the sensors and some limits in terms of possible location for the application.

In table 7.4 is indicated the distance of the measuring points tested by optical sensor (BOTDA system) and electrical sensors along the blade. The distance is calculated in function of the optical sensor, from the connecting point of the interrogator ("to sensor") to every single measuring point along the fibre (on the blade).

Measuring points (#)	Distances along the fibre on the blade (m)

56	25	30	101	66	161
23	28	26	108,5	28	170
27	38,5	22	118,5	32	180
31	47	53	128	36	197
64	48	55	135,5	71	198
67	49	20	147	37	215
35	60,5	62	148	33	226
39	75,5	65	149	29	236
72	76,5	24	159	25	245
38	77	63	160	21	256
34	91				

Table 7.4: Relation between points and distance along the fibre on the blade.

Because of restrictions imposed by the company, a precise characterization of the position of the measuring points along the blade cannot be revealed. However, a clearer and practical representation of the measuring scheme is illustrated in figure 7.4.

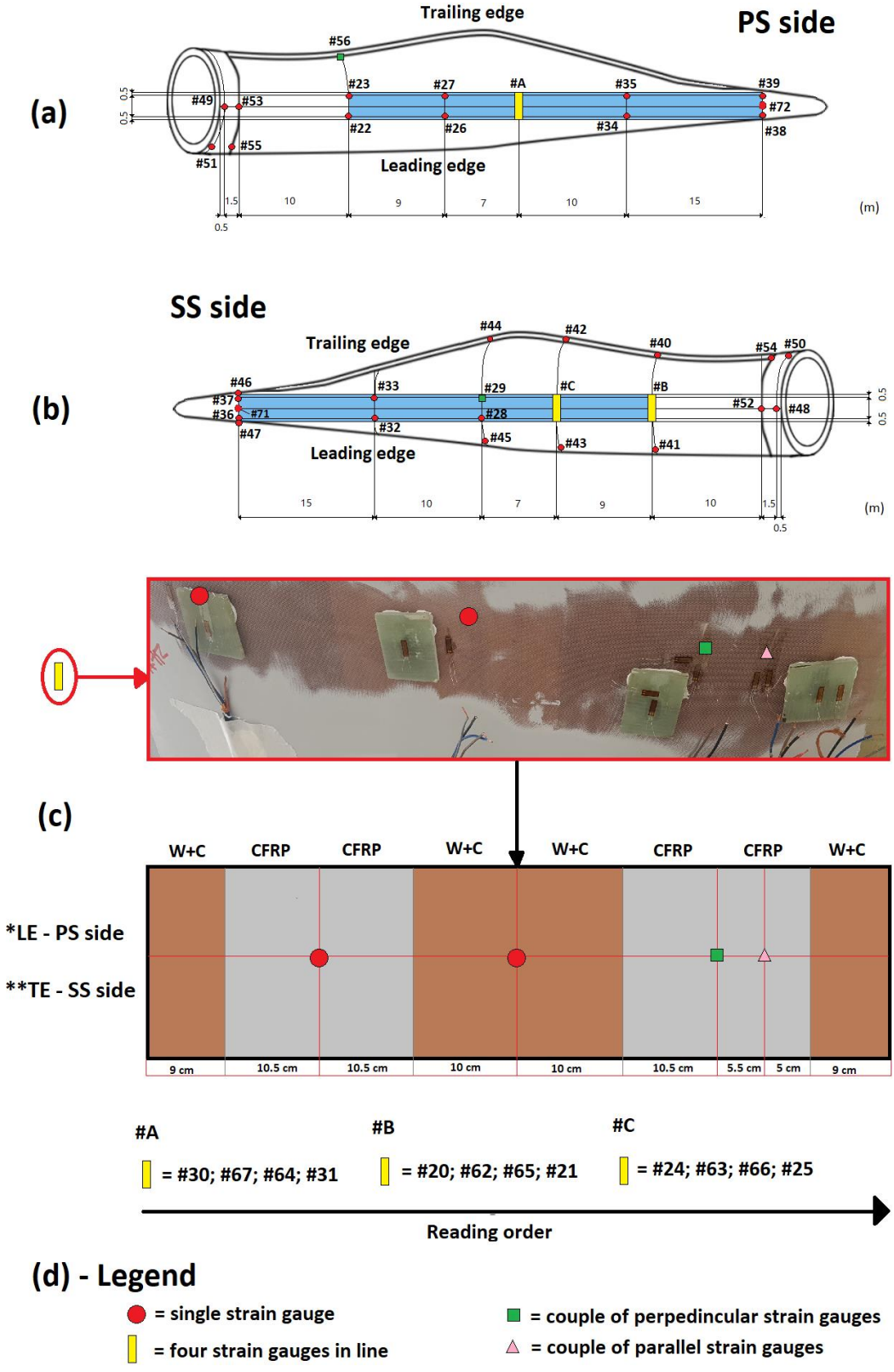

Figure 7.4: Visual disposition of the measuring points on the blade.

It might be helpful to the reader explaining some technical abbreviations that has not been introduced during the development of this chapter. “PS” means pressure side and “SS” means suction side.

Moreover, it is important to explain why there are couples of perpendicular strain gauges and couples of parallel strain gauges along the blade. The reason is because:

- In the first case, the company wants to measure the strain in both the directions (parallel and perpendicular to the direction of developing of the blade).
- In the second case it is has been considered that the point of interest is of crucial importance for the blade so in the case a strain gauge would not work, the other one could cover it and in the case they both work there could be a comparison between the values (understanding how the strain is locally developing).

The measuring operation might be divided into two main actions that are comparing some values obtained with strain electrical gauges, BOTDA, FBG and achieving measurements by using optical fibre, in the locations not reachable by the strain gauges.

As first, it is important to explain how the optical fibre systems have been carried out. The FBG optical sensing system has been completed with the following steps.

First, after the workers have marked the places where the electrical gauges should be placed, four stretching-elements have been assembled on the blade to enable the resistance test (the test has been conducted by using metal cables to connect the four stretching-elements to four stretching-organs). A representation of the result is as in fig. 7.5.

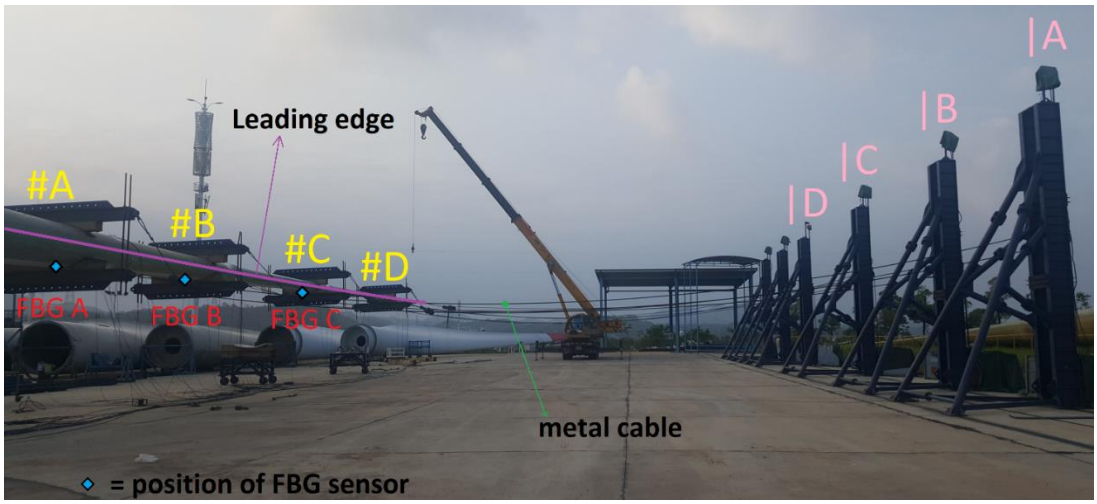

Figure 7.5: LE-edgewise-test setup.

The distance of the stretching-elements from the beginning of the blade are as following: #A - 18.864m, #B - 25.867m, #C - 35.883m, #D - 47.947m.

Before the assembling of the stretching-elements, 3 FBG sensors have been placed between #A, #B, #C (see figure 7.5). They are placed at the same distance as the stretching-elements, on the main beam of the blade at SS side.

Moreover, a combination of 6 FBGs (#1, #2, #3, #4, #5, #6) has been placed on the SS side of the blade. It has covered points #20, #65, #24, #63, #66, #28 (from FBG #1 covering #20, to FBG #6 covering

#28, the sequence is obvious). The 6 FBGs have been connected each other in an single optical waveguide, while FBG A, FBG B, and FBG C required each one a single optical waveguide, since the wavelength of the three sensors was similar and connecting them by a single optical waveguide might bring to a wrong mode of operation. The total FBG system is represented as in figure 7.6.

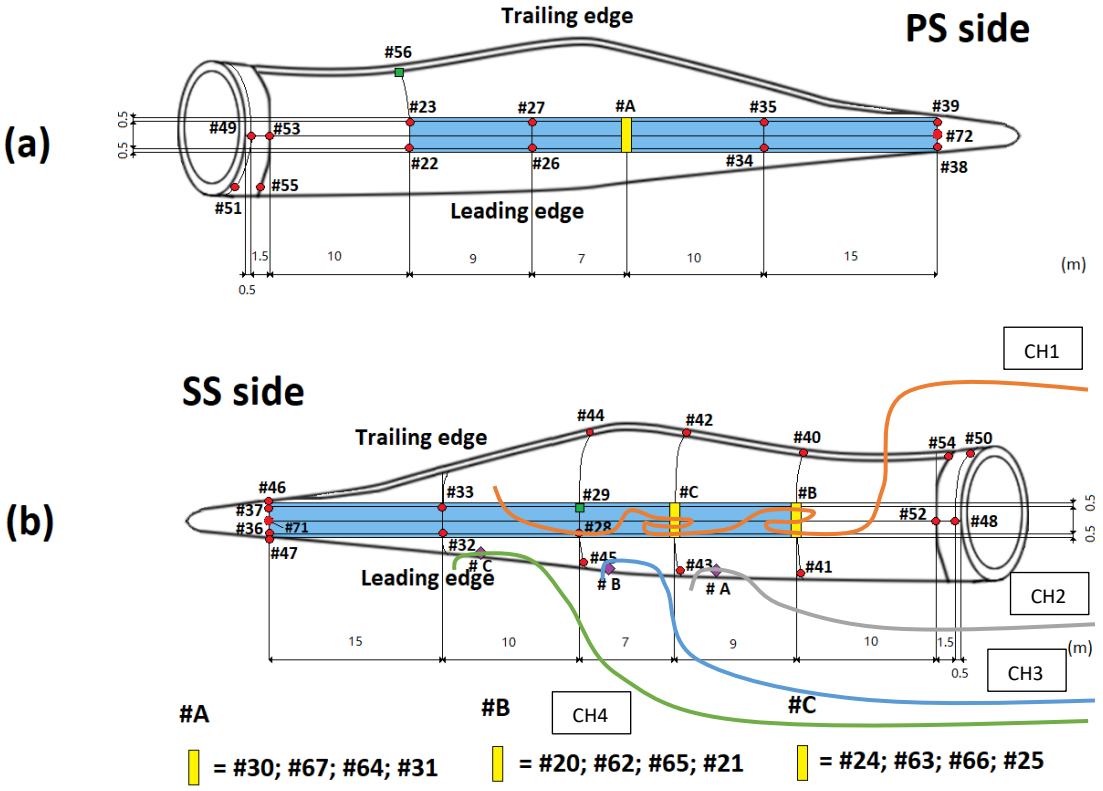

Figure 7.6: Disposition of the FBG sensing system on the blade.

Secondly, once the stretching-elements have been applied to the blade, the silicone-rubber coated optical fibre has been installed as in figure 7.7.

The BOTDA sensing system has been installed to cover all the points along the main beam of the blade and cover some points along the path that connects the SS side's main beam and PS side's main beam. The dotted line that connects PS side with SS side is only a visual solution, since in the reality the disposition of the blade is not as in figure.

Both the optical fibre-sensing systems have been installed using fibreglass tape for the long sections and Glue 502 for the short sections near the electrical gauges measuring points, since the sticking power of the glue is higher than the tape's one (ensuring then a safer and more accurate operation near the measuring points).

Differently from the FBG system, for BOTDA has been used only one fibre, connected in the beginning and in the end in one of the two channels of the DiTeSt interrogator.

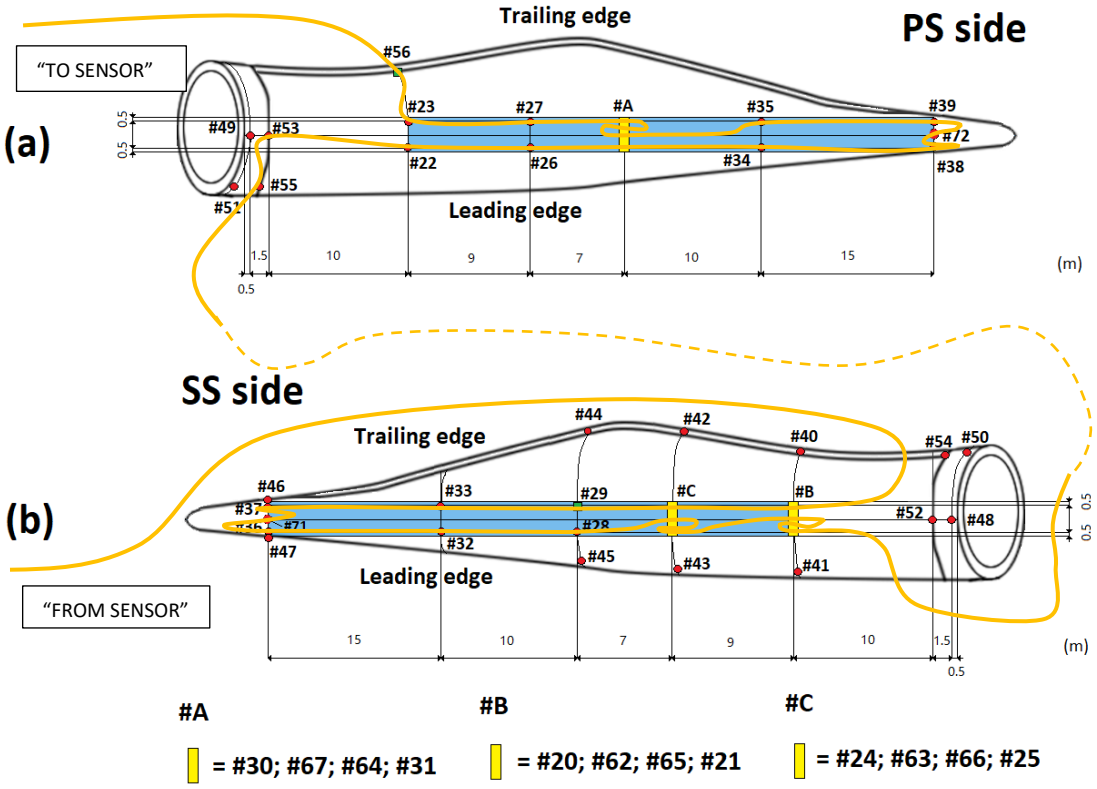

Figure 7.7: Disposition of the BOTDA sensing system on the blade.

7.4 - The test

The thesis will focus on a part of the total test that has been conducted by the company. The total test consisted of four experiments: stretching PS side, SS side, LE, and TE. In this elaborate the results will regard just the LE and the respective edgewise test. An illustration of the setup of the test is represented in figure 7.5.

The stretching-elements have been connected by metal cables to stretching powered organs that were automatically controlled. The loading-time parameters that have been used to control the machines are as in table 7.6.

Loading %	40%	60%	80%	100%
Stretching time (s)	200	100	100	100
Holding time (s)	30	30	30	10

Table 7.5: Loading-time parameters used to control the stretching machines.

The loadings are different test by test; for example, for the PS side, the loading will be higher than the loading in SS side, according to emulate the working conditions of the blade (PS side works with higher loadings since it is directly faced to the wind current).

7.4.1 - BOTDA results

BOTDA has been used to measure the static strain present on the blade during the holding periods. Its usage has been then limited during the total testing period. The DiTeSt interrogator parameters have been set in order to obtain a measurement that respects the time limits of the testing parameters (holding periods). The values of "Averaging cycles" and "Frequency step" of the interrogator have been adjusted to fit the limits.

The test steps are eight (and so the measurements):

1. Loading until 40% (in 200 s) and holding the load for 30 s.
2. Loading until 60% (in 100 s) and holding the load for 30 s.
3. Loading until 80% (in 100 s) and holding the load for 30 s.
4. Loading until 100% (in 100 s) and holding the load for 10 s.
5. Releasing until 80% (in 100 s) and holding the load for 30 s.
6. Releasing until 60% (in 100 s) and holding the load for 30 s.
7. Releasing until 40% (in 100 s) and holding the load for 30 s.
8. Releasing until 0% (in 200 s).

It is evident that the holding periods are all of 30 s (except just one of 10 s). This means that among the measurements taken with DiTeSt, seven were of 30 s, and one of 10 s. The beginning of the measurement corresponded to the beginning of the holding period and the end of the measurement corresponded to the end of the holding period.

The next eight graphs represent the data obtained with different loading conditions. They compare the values obtained by electrical gauges and BOTDA (in terms of strain) as a function of their position along the fibre. It is possible to refer to table 7.4 in order to understand the relation between distance and relative points.

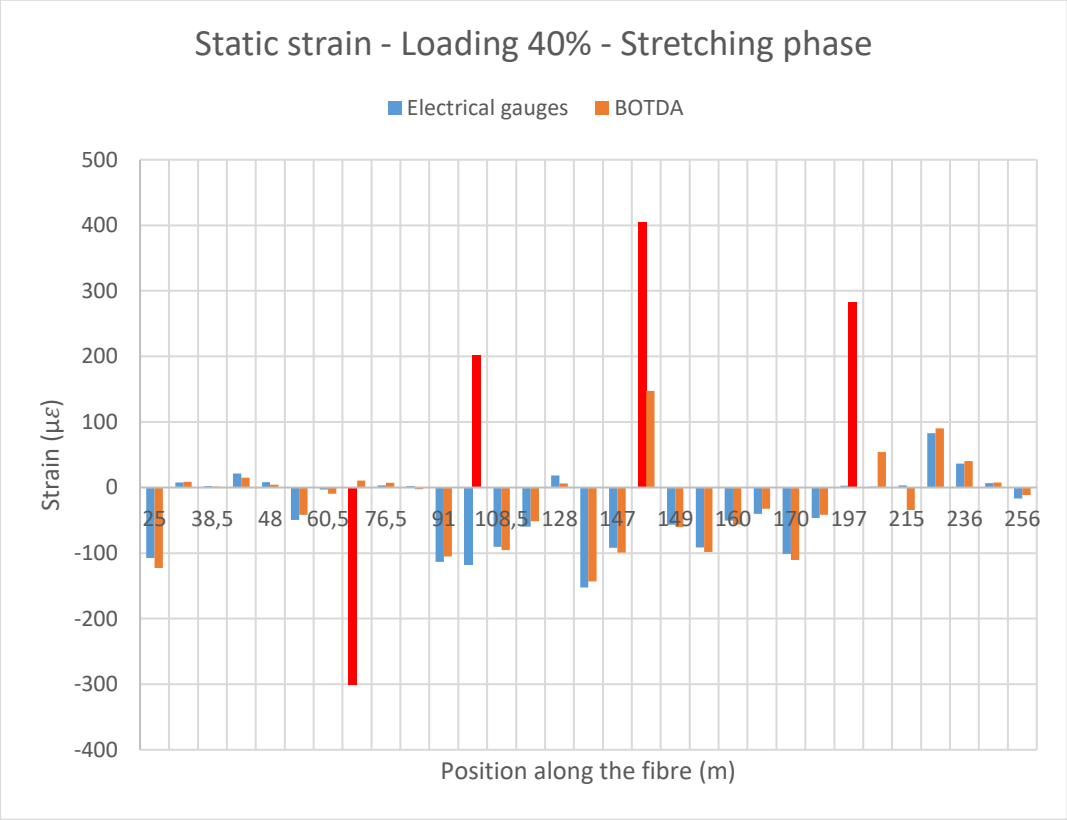

Figure 7.8: Loading of 40%, stretching phase, holding period of 30 s.

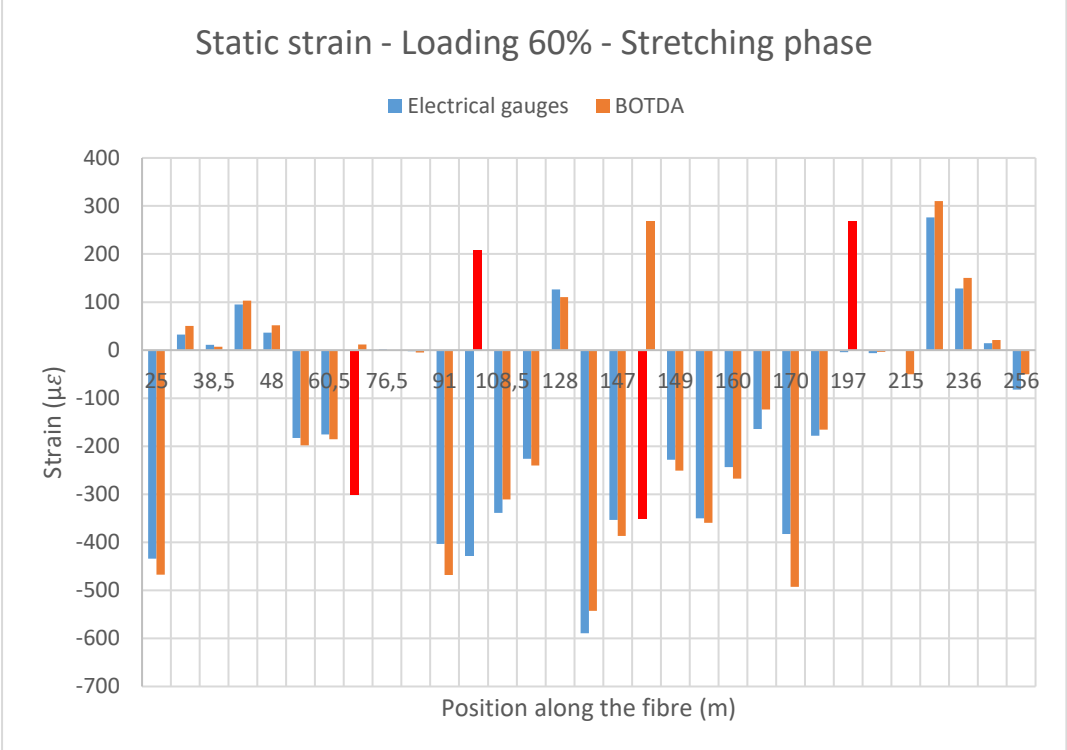

Figure 7.9: Loading of 60%, stretching phase, holding period of 30 s.

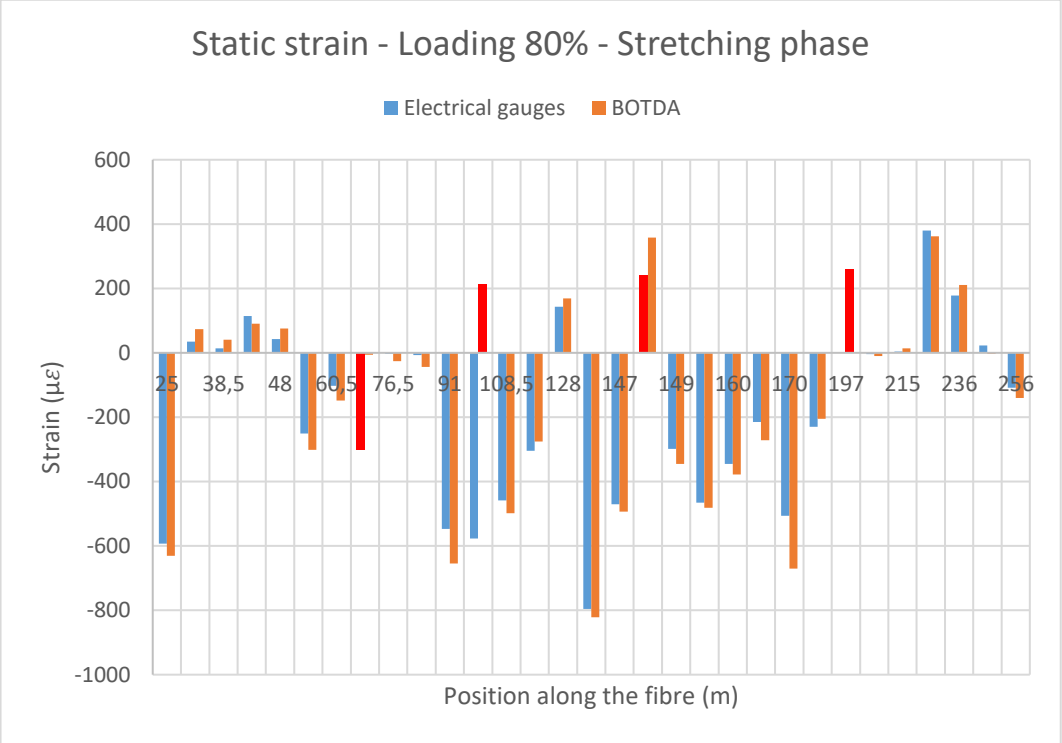

Figure 7.10: Loading of 80%, stretching phase, holding period of 30 s.

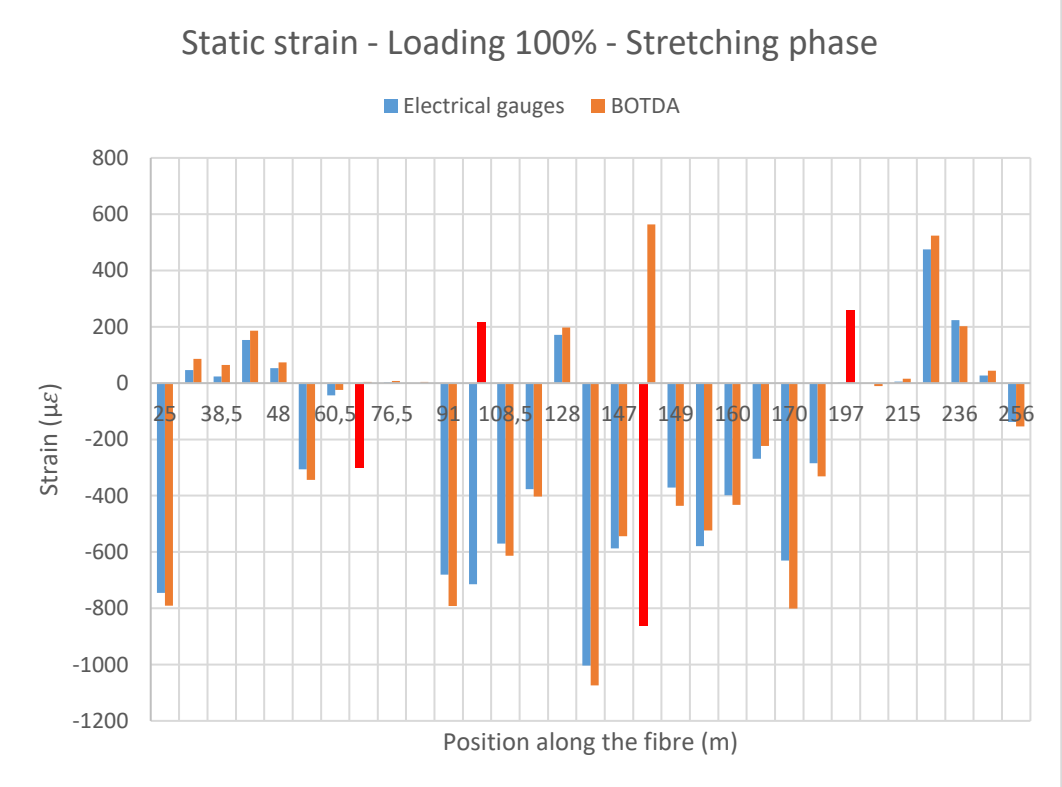

Figure 7.11: Loading of 100%, stretching phase, holding period of 10 s.

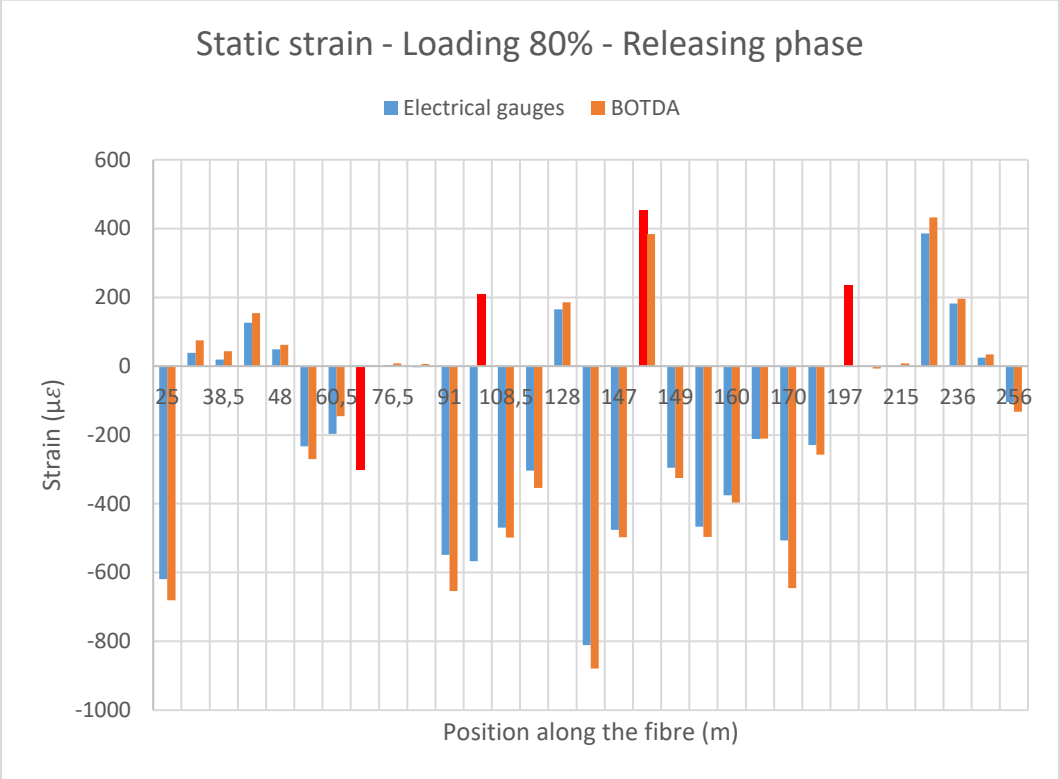

Figure 7.12: Loading of 80%, releasing phase, holding period of 30 s.

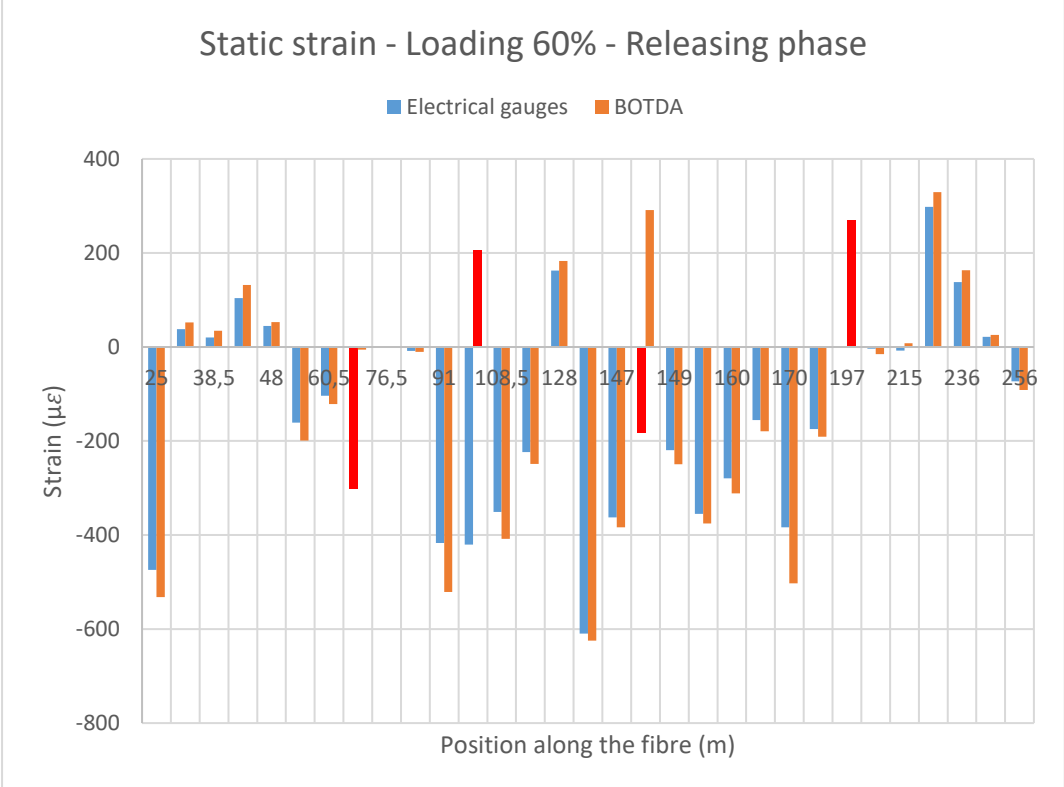

Figure 7.13: Loading of 60%, releasing phase, holding period of 30 s.

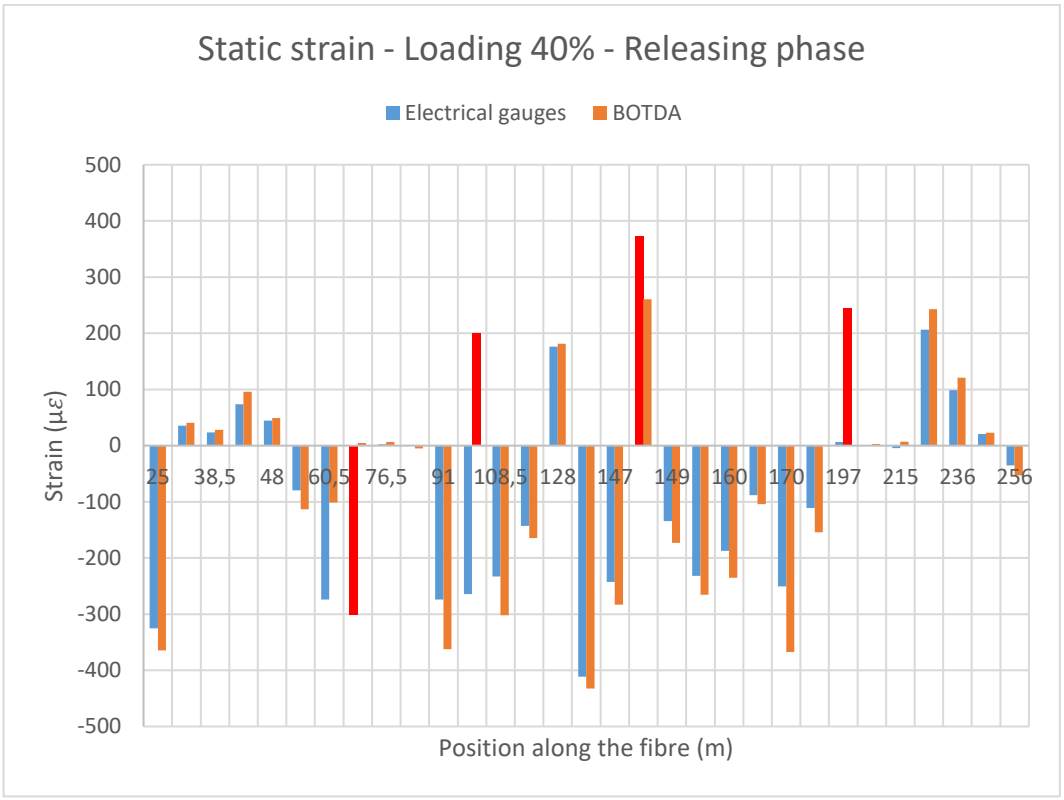

Figure 7.14: Loading of 40%, releasing phase, holding period of 30 s.

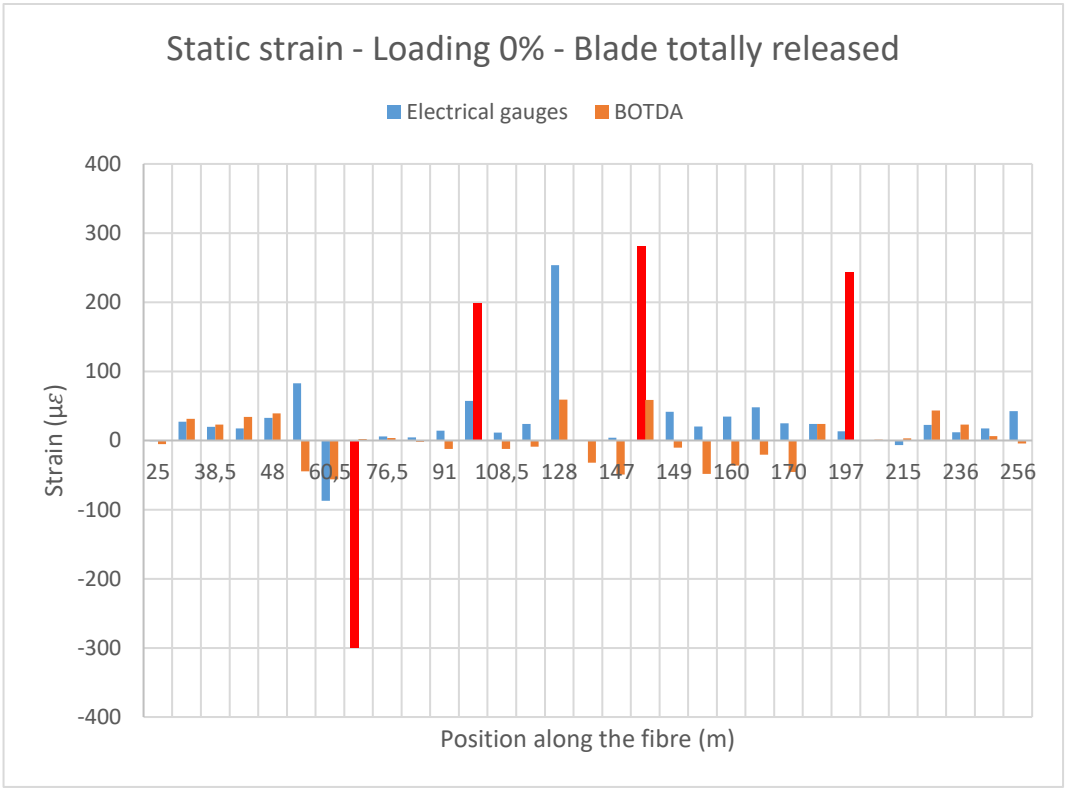

Figure 7.15: Loading of 0%, blade totally released.

The red line confirms that the values obtained with that specific sensor are wrong because of some technical or installation problems. According to the graphs, two electrical gauges and two parts of the distributed optical fibre gave unexpected (and wrong) results.

It is evident that for all the other points the difference is generally not high. The maximum difference is of 171 $\mu\varepsilon$ (that is around the 20% in percentage, referring to the strain measured by the electrical gauge), for point #28, with loading of 100%. On the other hand, especially when the strain values are low, the electrical gauges and optical fibre sensor values are almost equal. This does not mean that the values are surely right, but that there is accordance between the two sensors.

As discussed in the previous chapters, for optical sensing usually the measurement is not only related to the strain variation but also to the temperature variation. This means that the Brillouin frequency shift value gives in part information about the strain variation and in part information about the temperature variation. Actually, it would be impossible obtaining only one of the two values. The solution to overcome this problem is usually isolating a part of the fibre (for example covering it with a Teflon tube) in according to let the fibre itself loose inside the tube and unperturbed by the strain variations of the element where it is applied. As result, the compensation part should only contain information about the temperature. The covered part's position depends on the point that requires compensation. The compensated part should be near the measuring part or precisely reachable on the resulting data. Then the value related to the part of the fibre treated with compensation will be subtracted to the equivalent value that actually contains information about strain and temperature. Finally, the calculation of the strain of the measuring point should be completed.

During the experiment, the application of Teflon tube for compensation has resulted initially too arduous, since a big amount of Teflon pieces should be inserted as cover of the fibre, and be brought in each point, but the time was limited. A solution was found to overcome this problem: covering the fibre directly in the involved place with a paper cover, to emulate the effects of imperturbation of the Teflon tube.

Anyway, the experiment did not require the usage of this technique. The motivations are:

- The experiment period has been short (totally, less than twelve minutes). Therefore, the temperature variation was tiny.
- The weather has been cloudy for all the day, and the temperature was the same in each measuring point of the blade (if there were sun there could be a big difference between the upside and downside surface).

The measurement, with these working conditions, did not require the compensation, since the temperature variations were null. The auto-setup of the sensor has been done just before the beginning of the experiment, deleting then the temperature contribution to the obtained results.

7.4.2 - FBG results

The data obtained with FBGs have been dynamical. This means that the measurement describes the strain performance in function of the time. The BOTDA sensing system works with one fibre that gives a distributed measurement; this means that the measurement will be related to a specific time, but will develop in function of the position along the fibre.

The following graphs describe the trend of the strain from the beginning until the end of the test of the tested points. For the reasons discussed above, the measurement name will not be function of the loading, but function of the measuring point.

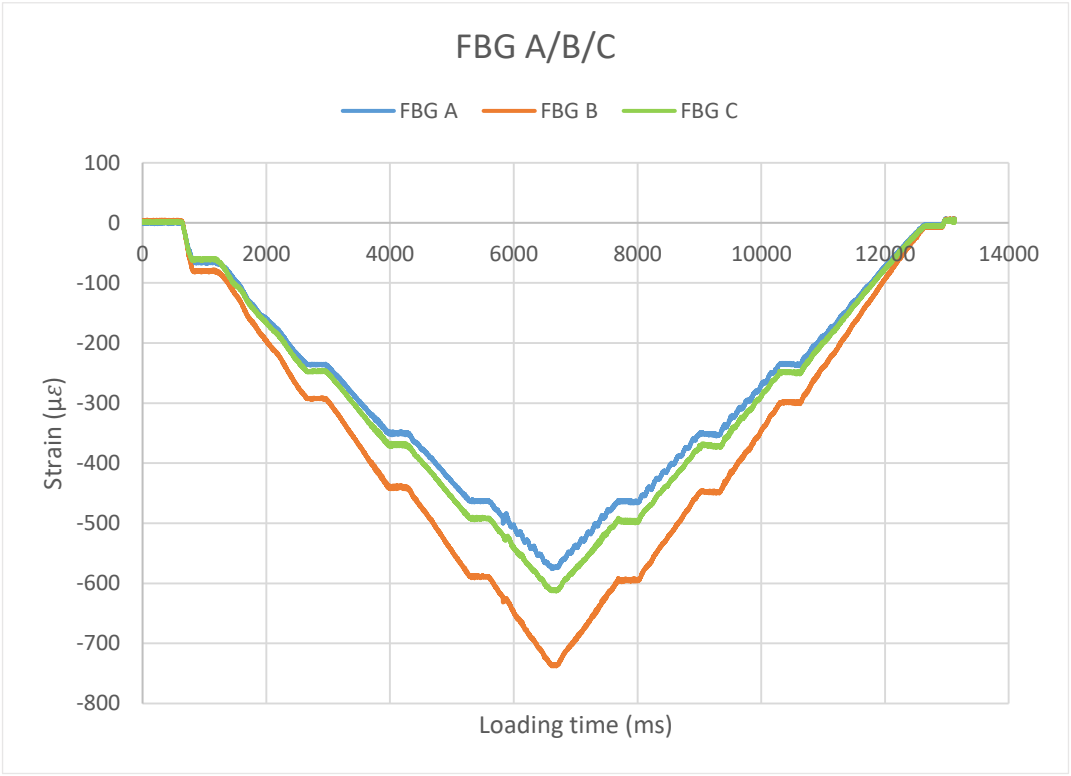

Figure 7.16: FBG A/B/C.

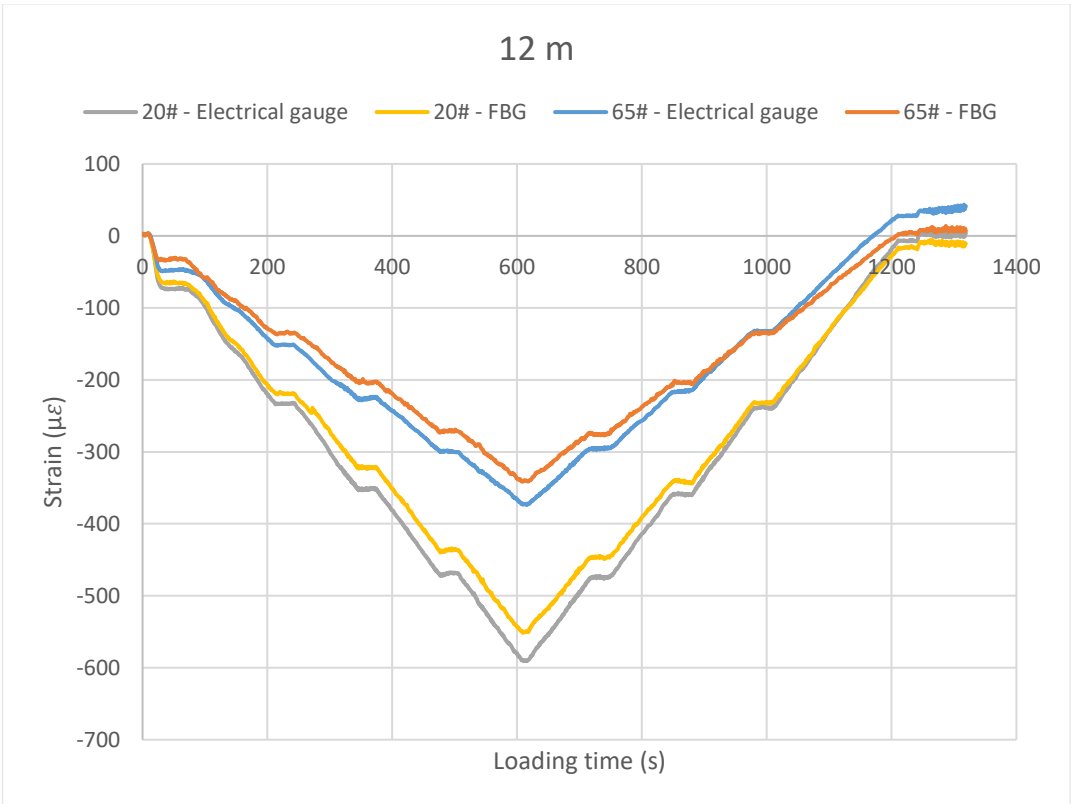

Figure 7.17: 12 m line.

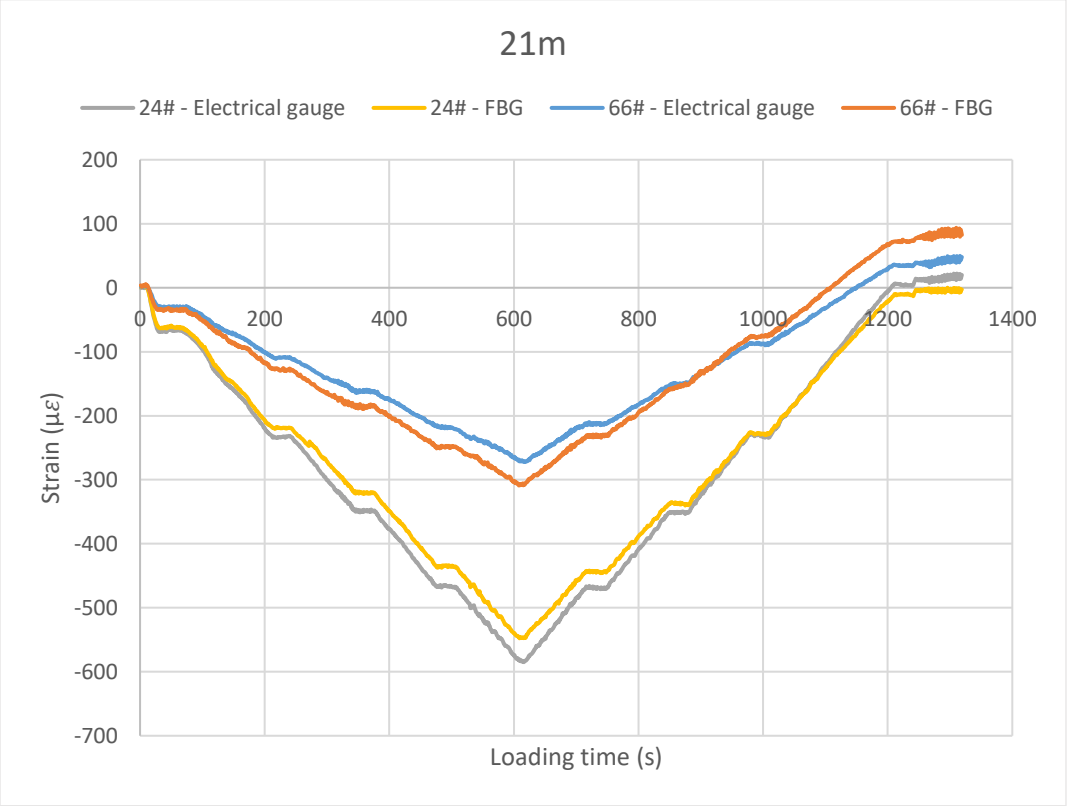

Figure 7.18: 21 m line (except 63#).

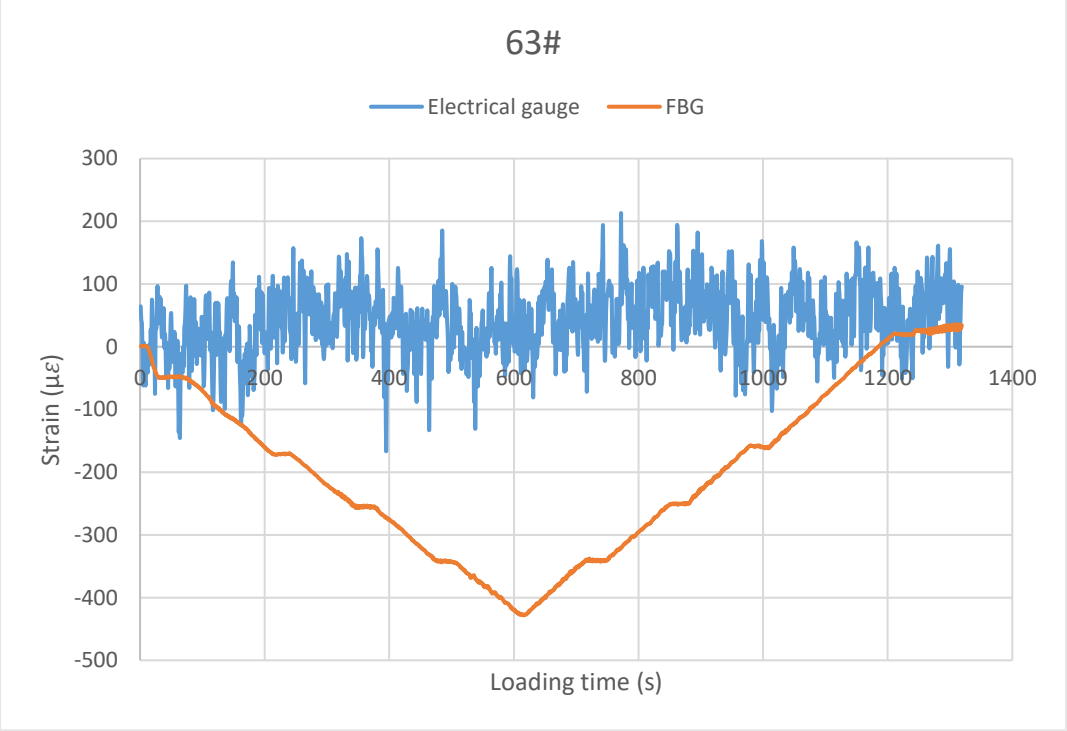

Figure 7.19: 63#.

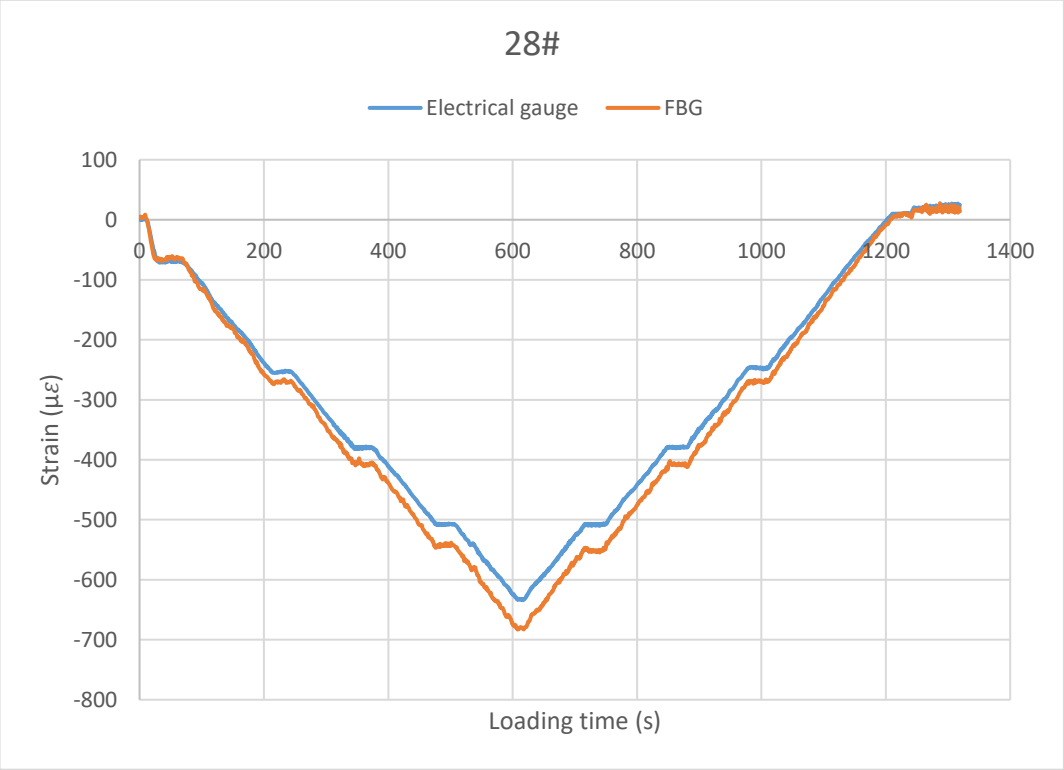

Figure 7.20: 28#.

For the stretching-elements A/B/C, the only used sensors were FBGs, as requested from the company. It is then not impossible to make a comparison with electrical gauges. According to what said by the company's engineers, the values are reliable.

The comparison of the other six FBGs with the equivalent electrical gauges gave good results, since the highest difference was less than 40 $\mu\varepsilon$ (that is around the 7% in percentage, referring to the strain measured by the electrical gauge), for 24#, at 100% loading. In general, for low values of strain, the values of both FBGs and electrical gauges were equal. The electrical gauge of measuring point 63#, did not work well, but the FBG covered its malfunction (see figure 7.19).

Even if for both BOTDA and FBG interrogator there are some coefficients that interpret the measurement giving as output strain or temperature (directly), both the quantities are always affected each other. The weather helped the measurement and, as it has been discussed for BOTDA, the compensation was not required for FBG either, once the auto-setup has been completed just before the beginning of the measurement (deleting the effects of the temperature).

Chapter 8

8 - Conclusion and future work

The aim of the thesis has been introducing and describing the optical fibres as sensing system for measuring the strain on a wind turbine blade. Two typologies of OFS have been used, but other options were available too. The choice depends on the requisites of the measurement.

It has been demonstrated that the OFS's results were comparable with the results obtained using the traditional electrical gauges. It is a considerable outcome, since the distances that needed to be covered were long, letting the application of the fibre complicated. Moreover, the BOTDA interrogator was sensible to big changes in strain along the distributed optical fibre and as result, initially the "Offset level" of the measurement was too low. After adjusting the disposition of the fibre along the blade, a high enough "Offset level" has been reached, enabling the achievement of a precise measurement.

The advantage is clear, since the complexity of using electrical gauges, which have to be connected electrically one by one with long, many, and heavy electrical cables is high. In the case of BOTDA, a single distributed optical fibre that once glued, is able to work and give a complete set of data along all the glued part, is expression of convenience.

After the experiment, the company that welcomed us accepted to have a long-term collaboration with the laboratory. The aim of the cooperation is projecting a SHM measuring structure where the optical fibres are inside the blade.

Since the system has to work also when the blade will be assembled on the turbine, in other words, when it is rotating with the turbine, the setup would be complex. The solution might be using rotating connectors, but it is not aim of the thesis developing this concept. Anyway, the usage of electrical gauges in this case might also be possible, but more complex, since there are more and more cables that would bother the blade during its moving or be object or breakage. Moreover, the cables would change the aerodynamic parameters of the blade, since their weight is not negligible. A last solution could be using wireless sensors, but since the measurement should be long in time, there could be some problems with power availability.

Bibliography

[1]: World Wind Energy Association, “Wind Power Capacity reaches 539 GW, 52,6 GW added in 2017”, *Press Releases,* Statistics, February 12, 2018.

[2]: Anindya Ghoshal, Mannur J. Sundaresan, Mark J. Schulz, P. Frank Pai, “Structural health monitoring techniques for wind turbine blades”, *Journal of Wind Engineering and Industrial Aerodynamics,* Vol. 85, pp. 309-324, 2000.

[3]: Del Campo, V.; Ragni, D.; Micallef, D.; Diez, F.J.; Simão Ferreira, C.J., “Estimation of loads on a horizontal axis wind turbine operating in yawed flow conditions”, *Wind Energy,* Vol. 18, 1875–1891, 2015.

[4]: Lars Pilgaard Mikkelsen, Leon Mishnaevsky Jr., “Computational Modelling of Materials for Wind Turbine Blades”, *Selected DTU Wind Energy Activities,* 8 November 2017.

[5]: Leon Mishnaevsky Jr., Kim Branner, Helga Nørgaard Petersen, Justine Beauson, Malcolm McGugan and Bent F. Sørensen, “Materials for Wind Turbine Blades: An Overview”, *Materials — Open Access Journal of Materials Science,* 9 November 2017.

[6]: Mikkelsen L.P., “A simplified model predicting the weight of the load carrying beam in a wind turbine blade”, *IOP Conf. Ser. Mater. Sci. Eng.*, 139, 2016.

[7]: Baumgart F., "Stiffness-an unknown world of mechanical science?", *Injury,* Retrieved 2012-05-04.

[8]: Jeff Kerns, “What’s the Difference Between Strain Gauges?”, *Machine Design,* September 21, 2017.

[9]: Bryzek, J., Roundy, S., Bircumshaw, B., Chung, C., Castellino, K., Stetter, J.R., Vestel, M., "Marvelous MEMS", *IEEE Circuits and Devices Magazine,* 22 (2): 8–28, 10 April 2006.

[10]: National Instruments Corporation, “Application Note 078”, *National Instruments,* 1998.

[11]: Geib, D., “Multiplexing of Extrinsic Fabry-Perot Optical Fiber Sensors for Strain Measurements”, *M.S. Thesis, Virginia Polytechnic Institute and State University*, 2003.

[12]: Fidanboylu K.a., Efendioglu H. S., “Fiber optic sensors and theri applications”, *5th International Advanced Technologies Symposium (IATS’09),* May 13-15, 2009.

[13]: N. Iftimie, R. Steigmann, N.A. Danila, D. Rosu, P.D. Barsanescu and A. Savin, “Wireless Sensors for Wind Turbine Blades Monitoring”, *IOP Conf. Series: Materials Science and Engineering,* 209 (2017) 012055.

[14]: Gangbing Song, Hui Li, Bosko Gajic, Wensong Zhou, Peng Chen and Haichang Gu, “Wind turbine blade health monitoring with piezoceramic-based wireless sensor network”, *International Journal of Smart and Nano Materials,* 4:3, 150-166, DOI: 10.1080/19475411.2013.836577, 25 Sep 2013.

[15]: Arthur H. Hartog, “An introduction to distributed optical fibre sensors”, *CRC Press, Taylor & Francis Group, Boca Raton – London – New York”,* 2017.

[16]: Brooks J., R. Wentworth, R. Youngquist et al., “Coherence multiplexing of fiber-optic interferometric sensors”, *J. Lightw. Technol.* 3: 5: 1062-1072, 1985.

[17]: Olshansky R., and D. B. Keck, “Pulse broadening in graded-index optical fibres”, *Appl. Opt.,* 15: 2: 483, 1976.

[18]: Martinelli M., "Time reversal for the polarization state in optical systems", *J. Mod. Optic.,* 39: 3: 451-455, 1992.

[19]: Krishnan R. S., "Temperature variations of the Raman frequencies in diamond", *Proc. Indian Acad. Sci. (Math. Sci.),* 24: 1: 45-57, 1946.

[20]: Song K. Y., Z. He, and K. Hotate, "Distributed strain measurement with millimeter-order : spatial resolution based on Brillouin optical correlation domain analysis", *Opt. Lett.,* 31: 17: 2526-2528, 2006.

[21]: Schroeder J., Mohr R., Macedo P., and Montrose C., "Rayleigh and Brillouin scattering in $K_2O - SiO_2$ glasses", *J. Am. Ceram. Soc.,* 56: 10: 510-514, 1973.

[22]: Fabelinskii I. L., "Molecular scattering of light", *Plenum Press, New York,* 1968.

[23]: Heiman D., D. S. Hamilton, and R. W. Hellwarth, "Brillouin scattering measurments on optical glasses", *Phys. Rev. B,* 19: 12: 6583, 1979.

[24]: Tkach R. W., A. R. Chraplyvy, and R. M. Derosier, "Spontaneous Brillouin scattering for single-mode optical-fibre characterisation", *Electron. Lett.,* 22: 19: 1011-1013, 1986.

[25]: Bommel H. E., and K. Dransfel, "Excitation and attenuation of hypersonic waves in quartz", *Phys. Rev.,* 117: 5: 1245-1252, 1960.

[26]: Maughan S. M., H. H. Kee, and T. P. Newson, "Simultaneous distributed fibre temperature and strain sensor using microwave coherent detection of spontaneous Brillouin backscatter", *Meas. Sci. Technol.,* 12: 7: 834-842, 2001.

[27]: Ohno H., Y. Uchiyama, and T. Kurashima, "Reduction of the effect of temperature in a fiber optic distributed sensor used for strain measurements in civil structures", *1999 Symposium on Smart Structures and Materials,* Newport Beach, CA, USA, SPIE 3670, 486-496, 1999.

[28]: Jones J. D., "Review of fibre sensor techniques for temperature-strain discrimination", *12th International Conference on Optical Fibre Sensors, Washington, DC, Optical Society of America, 16OTuC1,* 1997.

[29]: Parker T. R., M. Farhadiroushan, V. A. Handerek, and A. J. Rogers, "Temperature and strain dependence of the power level and frequency of spontaneous Brillouin scattering in optical fibres", *Opt. Lett.,* 22: 11: 787-789, 1997.

[30]: Vacher R., and J. Pelous, "Behavior of thermal phonons in amorphus media from 4 to 300K", *Phys. Rev. B,* 14: 2: 823, 1976.

[31]: DeSouza K., P. C. Wait, and T. P. Newson, "Characterisation of strain dependence of the Landau-Placzek ratio for distributed sensing", *Electron. Lett.,* 33: 7: 615-616, 1997.

[32]: Nikles M., "La diffusion Brillouin dans le fibres optiques: étude et application aux capteurs distribués", *PhD Ecole Polytechnique Fédérale de Lausanne,* 1997.

[33]: Galindez-Jamioy C.A., and J.-M. Lopez-Higuera, "Brillouin distributed fibre sensors: An overview and applications", *J. Sensors,* 2012. Article ID 204121, 2012.

[34]: Urricelqui J., A. Zornoza, M. Sagues, and A. Loayssa, "Dynamic BOTDA measurements based on Brillouin phase-shift and RF demodulation", *Opt. Expr.,* 20: 24: 26942-26949. 2012.

[35]: Eickhoff W., and R. Ulrich, "Optical frequency domain reflectometry in single-mode fiber", *Appl. Phys. Lett.,* 39: 9: 693-695, 1981.

[36]: K. O. Hill, Y. Fujii, D. C. Johnson, and B. S. Kawasaki, “Photosensitivity in optical fiber waveguides: Application to reflection filter fabrication,” *Appl. Phys. Lett.,* vol. 32, pp. 647–649, 1978.

[37]: B. S. Kawasaki, K. O. Hill, D. C. Johnson, and Y. Fujii, “Narrow-band Bragg reflectors in optical fibers,” *Opt. Lett.,* vol. 3, pp. 66–68, 1978.

[38]: Othonos Andreas, Kalli Kyriacos, “Fiber Bragg Gratings: Fundamentals and Applications in Telecommunications and Sensing”, *Artech House,* ISBN 0-89006-344-3, 1999.

[39]: Horiguchi T., and M. Tateda, “BOTDA – Nondestructive measurement of single-mode optical fibre attenuation characteristics using Brillouin interaction: Theory”, *J. Lightw. Technol.,* 7: 8: 1170-1176, 1989.

[40]: Horiguchi T., K. Shimizu, T. Kurashima, M. Tateda, and Y. Koyamada, “Development of a distributed sensing techinque using Brillouin scattering”, *J. Lightw. Technol.,* 13: 7: 1296, 1995.

[41]: Soto M. A., and L. Thévenaz, “Modeling and evaluating the performance of Brillouin distributed optical fibre sensors”, *Opt. Expr.,* 21: 25: 31347 – 31366, 2013.

[42]: Bao X., A. W. Brown, M. D. DeMerchant, and J. Smith, “Characterization of the Brillouin-loss spectrum of single-mode fibers by use of very short (10-ns) pulses”, *Opt. Lett.,* 24: 8: 510, 1999.

[43]: Dzulkefly Bin Zan M. S.,T. Tsuramaya, and T. Horiguchi, “The use of Walsh code in modulating the pump light of high spatial resolution phase-shift-pulse Brillouin optical time domain analysis with non-return-to-zero pulses”, *Meas. Sci. Technol.,* 24: 9: 094025, 2013.

[44]: Chaube P., B. G. Colpitts, D. Jagannathan, and A. W. Brown, “Distributed fiber-optic sensor for dynamic strain measurement”, *IEEE Sens. J.,* 8: 7: 1067-1072, 2008.

[45]: Voskoboinik A., D. Rogawski, H. Huang et al., “Frequency-domain analysis of dinamically applied strain using sweep-free Brillouin time-domain analyzer and sloped-assisted FBG sensing”, *Opt. Expr.,* 20: 26: B581-F586, 2012.

[46]: Hartog A. H., “Optical time domain reflectometry method and apparatus”, US6542228B1, 2003.